Trends and Challenges of Refractometric Nanoplasmonic Biosensors

M.-Carmen Estévez, Marinus A. Otte, Borja Sepúlveda, Laura M. Lechuga

Institut Català de Nanociència i Nanotecnologia (ICN2)

CSIC & CIBBER-BBN, ICN2 Building Campus UAB, 08193 Bellaterra (Barcelona), Spain;

Abstract

Motivated by potential benefits such as sensor miniaturization, multiplexing opportunities and higher sensitivities, refractometric nanoplasmonic biosensing has profiled itself in a short time span as an interesting alternative to conventional SPR biosensors. This latter conventional sensing concept has been subjected during the last decades to strong commercialization, thereby strongly leaning on well-developed thin-film surface chemistry protocols. Not surprisingly, the examples found in literature based on this sensing concept are generally characterized by extensive analytical studies of relevant clinical and diagnostic problems. In contrast, the more novel LSPR alternative finds itself in a much earlier, and especially, more fundamental stage of development. Driven by new fabrication methodologies to create nanostructured substrates, published work typically focuses on the novelty of the presented material, its optical properties and its use – generally limited to a proof-of-concept – as a label-free biosensing scheme. Given the different stages of development both SPR and LSPR sensors find themselves in, it becomes apparent that providing a comparative analysis of both concepts is not a trivial task. Nevertheless, in this review we make an effort to provide an overview that illustrates the progress booked in both fields during the last five years. First, we discuss the most relevant advances in SPR biosensing, including interesting analytical applications, together with different strategies that assure improvements in performance, throughput and/or integration. Subsequently, the remaining part of this work focuses on the use of nanoplasmonic sensors for real label-free biosensing applications. First, we discuss the motivation that serves as a driving force behind this research topic, together with a brief summary that comprises the main fabrication methodologies used in this field. Next, the sensing performance of LSPR sensors is examined by analyzing different parameters that that can be invoked in order to quantitatively assess their overall sensing performance. Two aspects are highlighted that turn

out to be especially important when trying to maximize their sensing performance, being 1) the targeted functionalization of the electromagnetic hotspots of the nanostructures, and 2) overcoming inherent negative influence that stem from the presence of a high refractive index substrate that supports the nanostructures. Next, although few in numbers, an overview is given of the most exhaustive and diagnostically relevant LSPR sensing assays that have been recently reported in literature, followed by examples that exploit inherent LSPR characteristics in order to create highly integrated and high-throughput optical biosensors. Finally, we discuss a series of considerations that, in our opinion, should be addressed in order to bring the realization of a stand-alone LSPR biosensor with competitive levels of sensitivity, robustness and integration (when compared to a conventional SPR sensor) much closer to reality.

Keywords

Optical biosensors, plasmonic sensors, nanoplasmonics sensors, bioanalytical applications, surface biofunctionalization

1. Introduction

Driven by the increasing need for sensitive, fast, cost-effective, low-reagent-consumption and ease-of-use biosensors for applications in the clinical and biomedical field, a myriad of biosensing configurations and devices have appeared in the literature during the last decades. In connection to this, a major unmet diagnostic demand is the necessity of reliable compact Point-of-care (POC) devices, which can provide instant results in any place at any time, offering the possibility of personalized care that may result in an improved health outcome. From the currently well-defined technologies, optical biosensors show unquestionable advantages as compared to other biosensing technologies, including high immunity to electromagnetic (EM) interferences, better stability in aggressive environments, and above all, the ability of providing label-free measurements combined with their potential for multiplexing and miniaturization, offering a great prospective for highly integrated devices. Among the different optical sensing platforms, those based on the use of plasmonic structures meet many of these benefits, and hence, are considered to be key components for the creation of advanced biosensing platforms.

Plasmonics is the field that studies the interaction of EM radiation with metals. Resonant coupling of optical waves to the free electrons of a metal can give rise to surface bound EM modes that are commonly referred to as Surface Plasmons (SPs). These plasmonic modes are typically excited at the interface of a noble metal and a dielectric, thereby complying to the SP excitation condition that demands the presence of two adjacent materials with oppositely signed optical constants. SPs exhibit their maximum field intensity at the metal-dielectric interface, while decaying evanescent waves penetrate into both adjacent media. The evanescent field that penetrates into the surrounding dielectric provides the SP with a sensing probe that is extremely sensitive to changes of the refractive index (RI) close to the metal surface. It is this property that is exploited when plasmonic structures are used as

refractometric sensing platforms: changes that occur in the vicinity of the metal-dielectric interface, such as the attachment or recognition of biomolecules, induce RI changes that alter the excitation conditions of the SP. These changes can be tracked over time, providing a measurable quantity for the label-free detection of biomolecular interactions. SPs generally come in two varieties: propagating SPs excited on thin metal films, commonly referred to as Surface Plasmon Polaritons (SPPs) or Surface Plasmon Resonances (SPRs), and Localized Surface Plasmon Resonances (LSPRs), the latter being SPs excited on sub-wavelength-sized metal nanoparticles (see Figure 1).

LSPRs provide metal nanoparticles with exemplified absorption- and scattering cross-sections at specific wavelengths, opening up a world full of bright and vividly colored nanostructures in the VIS and NIR region of the light spectrum. Theoretical interest in the optical properties of metal nanoparticles dates back to the 20th century [1]. However, it has not been until recently, that, accompanied by the eruption of nanotechnology, providing new methods to fabricate, structure and measure nanoscale materials, that nanoplasmonics has experienced an enormous experimental boost leading to a deeper comprehension of these light-metal interactions. As a consequence, the optical properties of metal nanoparticles have led to many new applications in either new or already existing fields of interest, such as photovoltaic devices [2, 3], nanophotonics applications [4], biomedical applications such as imaging, drug delivery, photothermal therapy and therapeutics [5, 6] and, of course, biomolecular sensing [7].

In contrast, propagating SPRs have been around for approximately half a century now, providing SPR-based biosensors with sufficient time to position themselves as a landmark label-free biosensing platform. Nowadays, the initial potential of SPR sensors has surpassed all expectations, establishing this sensing concept as a routine analytical instrument. Motivated by both its simplicity and versatility, its scope of applications has spread into a wide range. In this regard, affinity and kinetic studies or simple detection of compounds have met a systematic, easy, fast, real-time and usually sensitive manner to be

done. Its validity as a reference optical biosensor is reflected from the number of yearly publications covering application areas ranging from environmental monitoring and food quality to safety, and clinical diagnostics. The implementation of SPR imaging (SPRi) as an alternative SPR-based approach that promotes in-parallel analyses, has expanded its use into the pharmaceutical research and the overall medical field, with applications including high throughput screening, protein-protein interaction studies and drug discovery, amongst others. Besides, the continuous progress in physics, engineering, material science and nanotechnology has allowed the introduction of performance-enhancing modifications to conventional SPR sensor configurations. Of particular importance is the pursuit of improvements in the three most reported weaknesses of SPR biosensors: sensitivity, throughput capabilities and potential for miniaturization.

To this end, LSPR-based biosensing platforms are considered to be the next-generation plasmonic sensing platforms. Their inherent advantages over conventional SPR sensors are expected to fill in the gaps left open by SPR sensors. Judging by the exponentially increasing number of publications in this topic during the last decade (see Figure 2), it is not a surprise that the field of nanoplasmonic sensing has been subjected to a great scientific interest. So far, most effort has been directed towards the fabrication and development of the employed nanostructures, the evaluation of its physical and optical properties and its potential to perform biosensing, although this latter concept is typically limited to a proof-of-concept point of view.

In literature, several works have already extensively covered the field of refractometric LSPR sensing in a very extensive and general manner [8-10]. In this review, we mainly focus on the progress made in this field during the last 4-5 years, paying special attention to the use of refractometric nanoplasmonic sensors for real biosensing applications, while identifying the implications, requirements and pending challenges in order to achieve fully operative devices with appropriate levels of sensitivity, robustness

and integration potential, that can make them ultimately competitive with conventional SPR-based devices.

2. SPR Biosensing: Improving Performance and Design

Despite being the most widely used label-free optical biosensor, SPR sensors suffer from several limitations when compared with other optical label-free sensing techniques, which can be traced back to fundamental properties of SPRs. First of all, the penetration depth of a SPR´s evanescent field into its neighboring dielectric is typically hundreds of nm, thereby being much larger than typical sizes of biomolecules [11]. Hence, in some analytical and clinical areas where concentrations to be detected are particularly low or when the target structure is much smaller than this penetration depth, the molecules occupy only a fraction of this evanescent field that acts as a sensing probe, thereby offering a resolution for the detection of analytes that is typically not sufficient. Furthermore, the characteristic SPR wave-vector exceeds that of light traveling through the same dielectric. Excitation of SPRs is therefore only possible when this momentum mismatch is overcome, something that can be achieved by enlarging the wave-vector of the excitation light. Generally, this is accomplished by using a prism-coupled Kretschmann excitation scheme, making the sensor configuration significantly bulky. Upon addition of the microfluidics, optical components and other hardware, most commercialized SPR biosensors are still portable, but their size and weight is not optimal, and far from ideal for LOC or POC devices. Finally, the large propagation distances of SPRs (10-100 µm) limit the minimum sensing area, thus strongly reducing high-throughput capabilities for multiplexed measurements. Not surprisingly, much effort is being put in overcoming these that are considered the weakest points of these biosensors. In the following paragraphs an overview is given of recent works that point toward this direction.

Although highly useful for real-time detection and with a proven effectiveness in the monitorization and characterization of biomolecular interactions, the sensitivity of refractometric SPR sensors usually

ranges between 10^{-6}-10^{-7} refractive index units (RIUs) [11, 12] and a limit of detection (LOD) of approximately 0.5-1 pg/mm^2. In terms of concentration sensitivities, these values would correspond to LODs in the pM-nM range, when optimal surface biofunctionalization has been previously done and high-quality biological reagents are employed. This limited sensitivity, which can be beaten by other label-free optical configurations [13], becomes a more critical factor for the direct detection of small analytes at very low concentrations, for clinical application where the concentrations can range from pM to fM, or for single-molecule detection. Most of the proposed strategies to overcome this problem tend to be based on the expansion of the detection assay with additional steps, such as the addition of successive reagents or compounds in a specific layer-based system. These approaches induce an overall increase of molecular weight and hence, a significant enhancement of the measured signal. An illustrative example comprises sandwich formats where secondary recognition elements are added, either free or labeled with for instance a nanoparticle [14-19]. Despite the improved sensing performance, this methodology complicates overall procedures, since more reagents are required, and analysis times are inevitably lengthened.

In the case that simplicity and rapidity are considered to be essential features, sensitivity enhancing strategies that affect the optics, the metallic surface, or the SPR excitation methodology, might be much more appropriate. For an extensive overview on these different approaches, we refer to the work carried out by Homola *et al.* [11]. The use of alternative SPR excitation methods, different from the conventional prism-based coupling scheme, such as the use of waveguide-[20, 21], fiber-optic-[20, 21], or grating-based light-coupling [22], have been considered as sensitivity enhancing strategies [23]. However, a recent theoretical study demonstrated that the sensitivity of SPR sensing is reaching its limit regardless of the employed coupling configuration and/or modulation technique (wavelength, angle, intensity) [24]. This work proclaims that most improvements may come from the optimization of the SPR itself, that is, by changing properties of either the employed thin metal films, or their dielectric

surroundings. To this end, it has been demonstrated that the use of multilayers built out of noble and ferromagnetic metals (Au/Co/Au), which exploit magneto-optical activity in combination with SPRs, result in a significant four-fold enhancement of the sensing performance of a conventional SPR biosensor [25, 26]. Also, Long-Range Surface Plasmon Resonance (LR-SPR) sensors have proven pronounced sensitivity improvements, reaching values of approximately $2.5 \cdot 10^{-8}$ RIU [27]. Compared to conventional SPR sensors, where the metal substrate is comprised between different dielectrics, LR-SPRs can only be excited when the thin metal film is comprised between two dielectric media with similar RI (i.e. the sensing medium - typically being the buffer used for biosensing applications - and a thin layer of Teflon). LR-SPRs propagate along the metal film exhibiting much larger penetration depths (200-1400 nm), which becomes especially relevant for the detection of large targets such as cells and bacteria yielding 2.5- to 5.5-fold better sensitivities [28], or to deeply study cellular response such as cell volume changes [29].

Also the microfluidics and the sample transport to the gold sensing surface have a strong impact on the sensing performance in terms of sample dispersion and overall response time. Homola's group has designed a dispersionless microfluidic system which minimizes the mixing of samples and enhances the sample transport directly to the surface by incorporating two pairs of in- and output ports for sample injection. Controlled valve-mediated port-switching allows for the regulation of the sample injection, assuring that the change of sample volumes takes place near the sensing surface [30]. These modifications improve the sensing performance, exhibiting a RI resolution of $1.3 \cdot 10^{-7}$ RIU [31]. Application of this strategy to oligonucleotide hybridization assays has led to a significant detectability improvement when compared to traditional microfluidics, achieving LODs as low as 70 pM [30], while its successful implementation has also been expanded to protein detection in diluted plasma [31, 32]. Besides, as recently demonstrated by Lynn *et al.*, geometrical aspects of the flow cell, such as the channel height, can also have a pronounced impact on the sensitivity of SPR sensing [33]. Finally, by

decreasing the size of the read-out area to a minimum, Kvasnička *et al.* have shown that the LOD can be pushed down to detection levels of a few hundreds of molecules [34].

Next to sensitivity-enhancing strategies, much interest is also still focused on the improvement of the multiplexing and miniaturization capabilities of these sensors. SPR sensors can be noticeably miniaturized and/or integrated if the prism-coupled excitation scheme is replaced by one of the previously mentioned alternatives such as dielectric waveguides, end-fire coupling, or diffraction gratings grafted into the plasmonic substrate. Nevertheless, each of these methodologies adds more complexity to both the fabrication process and the user-friendliness of the device. Other strategies that proclaim smaller and more integrated devices include those that leave out the pump that delivers solutions to the flow cell (an external pump is still necessary), or the use of integrated microfluidics. The latter option not only leads to more compact devices, but also opens up possibilities to improve the sensor´s capabilities to carry out multiplexed measurements. In this line, some of the reported SPR sensors incorporate several measurement channels [11], although most of them are limited to at most 10 channels. A second approach that provides the ability of carrying out multiplexed measurements is embodied by the SPR imaging (SPRi) concept [35, 36]. This technique, which is considered a large qualitative step forward in the field to microarray-based sensing, has become a valuable tool in proteomics, facilitating the simultaneous analysis of hundreds of biomolecular interactions. Essentially, a SPRi consists of an expanded light source projected onto a patterned gold surface, where the reflected light is imaged onto a CCD camera. Image processing algorithms allow for real-time contrast measurements of all the active spots, providing a quantitative measure for the amount of adsorbed molecules (refractive index change) on each sensing area. Different SPRi instruments are currently commercialized but, unfortunately, the sensitivity of these devices appear to be typically lower than the conventional SPR biosensors [24], and eventually, amplification steps are included in order to enhance the detectability. From a practical point of view, SPRi instruments commonly have restrictions in terms

of sample delivery, since they are limited to a single analyte/solution flown at a time on a multiple-ligand spotted surface. The use of appropriate microfluidics facilitate the evaluation of parallel and simultaneous analyte solutions and in case of being highly required, for internal referencing [37]. A few attempts have been done in order to develop microfluidic flow cell arrays with the aim of performing parallel and individualized throughput delivery. Eddings *et al.*[38, 39] have developed a 3D microfluidic flow cell array for the independent delivery of up to 48 different analyte solutions, either for the in-situ patterning of the spot or for the secondary delivery of the target solutions. More complex is for instance the flow cell developed by Ouellet *et al.* [40] consisting of a PDMS microfluidic flow array of 264 independent chambers with individual volumes of up to 700 pL. This system is also designed to allow for the recovery of bound sample for further downstream processing. Recently, both nanostructures and a digital droplet-based 2D microfluidic interfaces have been combined in a SPRi, to enhance both sensitivity and improve the automation of simultaneous analyses requiring ultra-low sample volumes [41-43].

3. Nanoplasmonic Biosensing

3.1 Motivation, Instrumentation and Fabrication

One could argue that the current increase in interest in nanoplasmonic sensing platforms is nothing more than the logical consequence of nanotechnology pushing conventional SPR sensing towards new frontiers. Either way, the most important question that needs to be answered is whether this evolution is worth the effort. Inherent benefits of metal nanostructures offer possibilities that can difficultly be met by conventional SPR sensors. Compared to SPRs, where the propagating nature of the plasmonic mode assures large effective sensing areas, the strong EM field confinement and the localized nature of LSPRs limits the minimum sensing area of metal nanostructures to their size. Combined with the

possibility of exciting the LSPRs with direct EM illumination, and thus becoming unnecessary the use of bulky coupling methodologies, the use of metal nanoparticles offers very promising opportunities for sensor miniaturization and multiplexing. Besides the strong EM field confinement of LSPRs ensures smaller penetration depths of the evanescent field into the surrounding dielectric. As a direct consequence, biomolecules attached to the nanoparticle surface occupy a much larger fraction of the evanescent field, raising the expectations of exceptional sensitivities for the detection of tiny biomolecules in low amounts.

In general, a nanoplasmonic biosensor consists of a nanostructured substrate with compatible microfluidics. The LSPR of the nanostructures can be excited by a UV-VIS light source, while a spectrometer collects the necessary light. For high nanostructure surface densities, extinction measurements are the easiest way to characterize the optical properties (See Figure 3.A). In this case, light is shed on the plasmonic nanostructures and the transmitted light is analyzed with a spectrometer. However, in the limit of single particle sensing, a much higher contrast is needed between the excitation light and the light absorbed by the nanoparticles. In those cases, scattering measurements are preferred. These high signal-to-background levels can be achieved by dark-field (DF) microscopy or total internal reflection (TIR) spectroscopy. As the size of the particles is reduced, the scattering cross section becomes smaller and absorption becomes dominant, making extinction measurements more desirable. In DF microscopy (transmission configuration) a DF condenser is used to focus a hollow – high numerical aperture – cone on the nanostructured substrate. Then, the scattered light dispersed by the nanostructures can be collected by a microscope objective with a lower numerical aperture (Figure 3.B). In contrast, in TIR microscopy, the LSPR is excited in a prism-coupled TIR configuration (Figure 3.C), thereby also using a microscope objective to collect the scattered light, but, in this case, without any restriction on its numerical aperture.

Nanostructured substrates employed in the nanoplasmonic biosensors can be divided in those based on *top-down* or *bottom-up* fabrication methodologies. While the former group relies on lithographical patterning techniques, the latter one is based on chemically synthesized colloidal nanoparticles that are further deposited on substrates. Herein, we only point out the basics of both fabrication concepts. For a more detailed and extensive information on the fabrication of nanoplasmonic structures, we refer to the review by Jones *et al*. [44]. The current variety and extraordinary optical properties of synthesized nanoparticles can be attributed to great advances in nanotechnology, providing researchers with the necessary wet chemistry methods that enable precise geometrical nanoparticle engineering. In this regard, next to spheres [45], rods [46-48], plates [49], triangles [50, 51], (bi)pyramids [52-54], cubes [55, 56], tubes [57], stars [58] or prisms [59], also hybrid- and alloy nanoparticles have been fabricated [60], such as for example core-shell particles [61-64], nanoflowers [65] or nanorice [66]. In all these cases, the nature of colloidal nanoparticles imposes serious drawbacks on their use as biosensors in solution (i.e. colorimetric aggregation-based assays). Changes in the ionic strength, pH or buffer temperature, can lead to the particle precipitation. Besides, surface biofunctionalization protocols can screen or modify the charge distribution yielding a rupture of the colloidal equilibrium. To avoid these difficulties, attachment of the colloidal nanostructures to a solid support can be the best alternative or even a prerequisite. An additional benefit is its compatibility with microfluidics for in-flow sensing assays. To this end, different methodologies have been developed that aim at attaching the colloidal nanoparticles to previously functionalized surfaces via either covalent or electrostatic linkage strategies. Thiol- or amino- modified glass surfaces can strongly attach gold nanoparticles to the surface, although sometimes this functionalization step can be especially tricky with particles that require a stabilizer layer on the surface to avoid aggregation, like in the case of nanorods, nanoplates or other kind of structures [49, 54]. These surface modifications usually hinder an efficient and reproducible coverage of the solid support. In an attempt to overcome this problem, additional steps are typically required involving the

exchange of this protective layer with other functionalized compounds (i.e. PEGylated compounds, thiolated compounds with carboxylic acid, biotin, etc). This step subsequently allows for binding to appropriately modified surfaces (amino-, thiol-, avidin-modified or opposite-charged surfaces so that electrostatic interactions occur [58, 67, 68]). An attractive alternative consists of directly growing the nanostructure on the substrate [69]. The surface density of immobilized nanoparticles can be controlled by optimizing parameters such as the concentration of the colloidal nanoparticle solution, the incubation time, or the temperature, making it possible to obtain highly-dense or very sparse surface concentrations. For sparse density, inter-particle discrimination becomes possible, enabling the spectral monitoring of a single nanostructure. It should be noted that almost all these immobilization strategies lead to a random nanoparticle surface distribution, yielding low control of both position and orientation. This issue can be overcome by carrying out a previous ordered functionalization of the substrate, for instance, by carefully modifying the surface at specific positions that finally results in an arrayed-based distribution.

The most typical top-down fabrication approaches include conventional lithography such as photolithography, electron beam lithography (EBL) or focused ion beam lithography (FIB), allowing for the formation of ordered arrays of nanometric structures with well-defined shapes and sizes. Although widely used, these techniques are slow and high-cost, and despite high levels of resolution, typically limit the patterning area to only a few μm^2. On the other side, conventional photolithography permits faster, parallel and large-scale fabrication at the expense of lower resolution. A different approach for large-scale and low-cost creation of plasmonic nanostructures is offered by colloidal lithography techniques, such as nanospheres lithography (NSL) [70-72], or hole-mask colloidal lithography (HCL) [73]. In both methods, the self-assembled layer of nanospheres onto the substrate is used as a sacrificial mask for the generation of nanostructured substrates. With NSL, hexagonal self-assembly of nanospheres in close-packed layers renders highly ordered patterning, whereas HCL, characterized by

short-range ordered arrays of nanostructures, offers more versatility in terms of particle geometry. Another fabrication methodology that currently receives much attention is nanoimprint lithography. This technique relies on the use of reusable master stamps, which can be either hard (rigid) [74], or soft (elastomeric) [75], that are used to imprint or transfer predefined patterns onto almost any desired substrate. These patterns are typically used as a mask for successive fabrication steps. Due to the reusability of the master stamps, and even their tunability in the case of soft stamps [76], nanoimprint lithography is considered a low-cost technique with potential for high-throughput fabrication of sub-micron structured substrates. Using this fabrication methodology, large nano-patterned areas of domes [77], cavities [78], holes [79], and dots/disks [80-82] have been reported. A different approach is offered by nanostencil lithography. Based on shadow mask deposition, and having the additional benefit of not requiring any resist-processing, baking, or solvent-use, this technique fabricates dense nanostructured substrates with high resolution [83], such as nanodots [84], or nanorods[85], and can even be extended for the creation of nanoplasmonic structures on flexible substrates[86, 87]. Next to these abovementioned approaches, other top-down methods that are worth mentioning include the use of porous alumina templates for the creation of vertical nanorods [88] and nanotubes [89], the direct seed-mediated growth of nanoplates directly on top of surfaces [69], the use of interference lithography [90], or the creation of nanoparticle cluster arrays using a hybrid top-down/bottom-up approach [91].

3.2 Sensing Performance of Refractometric LSPR Biosensors

3.2.1. Sensitivity Considerations

The ability with which metal nanostructures can detect RI changes is generally expressed in terms of their bulk sensitivity η_B, that is, the linear dependence of resonance wavelength λ_{LSPR} on the homogeneous bulk RI changes of the dielectric environment:

Next to η_B, a second property that strongly influences the sensing performance is the ability with which these spectral shifts can be discriminated, something that is normally taken into account by considering the full-width-half-maximum (Γ) of the resonance peak. Both quantities are often combined in a generalized performance-assessing figure-of-merit (FOM) parameter, defined as:

—,

This parameter, both valid in wavelength and energy scale [92], provides an easy way for the performance assessment of nanoplasmonic structures whose spectral response is described by a Lorentzian peak. However, to expand its use to other nanometric structures that exhibit more complex spectral responses, Becker *et al.* proposed an alternative *FOM*-quantity by considering relative peak intensity changes at the wavelength where the slope $dI/d\lambda$ is maximized [93]:

Both η_B, FOM_B and FOM_B* parameters are extensively used and considered to be good indications for the bulk sensing performance of nanoplasmonic sensors [78, 92-99]. Depending on the specificity of the employed sensing platform, different, but equally useable FOM definitions can be found. In this regard, Offermans *et al.* devised a generalized scaling law for lattice-based nanoplasmonic sensing schemes, in which the employed FOM parameter is uniquely determined by geometrical lattice properties [100].

However, from a biosensing point-of-view, it is much more interesting to probe the EM field distribution of a nanoplasmonic sensor close to the metal surface, which is the region where the biomolecular interactions take place. For this, a surface sensitivity parameter η_S can be defined that accounts for the near-field sensing performance:

In this expression, $d_,$ is the thickness of a very thin adsorbed layer that homogeneously coats the metal nanostructure, with a refractive index that is representative for organic molecules. Again, the accompanying figure-of-merit can be defined by: $FOM_S = \eta_S / \Gamma$, which in the limit of $d \rightarrow 0$ can be used to mutually compare the surface sensing performance of different (nano-)plasmonic sensing schemes. When considering the simplest type of metal colloids, the most archetypical example of a nanoplasmonic sensor is based on spherical gold nanoparticles. However, the strongly blue-shifted LSPR inherent to this particle-shape ($\lambda_{LSPR} < 600$ nm) results in a spectral overlap with the interband transition of gold. As a consequence, sensors based on spherical nanoparticles not only exhibit low bulk sensitivities ($\eta_B < 120$ nm·RIU^{-1}), but also broad peak widths ($\Gamma > 100$ nm) [101]. The resulting FOM parameters, which are an order of magnitude smaller than those corresponding to SPR sensors, limit their potential use as label-free refractometric LSPR nanobiosensors.

In contrast, a much better sensing performance is obtained when rod-shaped nanostructures are considered. For these particles, variation of their longitudinal axes allows for the spectral tuning of their LSPR, while maintaining relatively low particle volumes [102]. Red-shifting of their plasmon resonance not only assures larger sensitivities, but also distances their LSPR from the interband transitions of the employed plasmonic material. The combination of both factors results in enhanced bulk and surface sensing performances when compared to spherical nanoparticles. However, most interestingly, it has been shown that although conventional SPR sensors outclass these gold rod-shaped LSPR sensing platforms in bulk sensing performance by approximately one order of magnitude, their surface sensing performance dictates a very different behavior: gold nanorods exhibit a surface sensing performance that is 15% better than that of their SPR-counterpart, while theoretical calculations predict an even larger improvement [92]. Besides, nanorods exhibit an optimized spectral sensing region when their

aspect ratios lies between 3 and 4 (λ_{LSPR} = *700-800 nm*), which can be accessed through precise nanoparticle engineering [92, 93, 103]. Moreover, the overall sensitivity enhancement of single rod-based LSPR sensors can be duplicated when silver is used as the plasmonic material[47], although silver has the strong disadvantage of its chemical instability. These results not only demonstrate the potential of LSPR sensors, profiling them as alternative for conventional SPR sensors, but also emphasize the fact that when comparing both plasmonic sensing schemes, distinction between bulk and surface FOMs is mandatory. This discrepancy finds its roots in the different EM field distributions of both plasmon types. Due to the much larger penetration depths of SPRs into the surrounding dielectric, SPRs possess much larger sensing volumes for the detection of bulk RI changes. However, when it comes to biosensing, the spatially more confined EM field distribution of LSPRs assures a larger fractional occupancy of molecules, assuring better surface sensing performances. For a real comparative study involving both sensing platforms, only an assessment based on the surface sensing performance paints a realistic picture of the actual biosensing performance.

Unfortunately, different nanoparticles are usually compared through their bulk sensing performance, often leaving their surface sensing characteristics out of the equation. For conventional spheroidal nanostructures, such as spherical and rod-shaped particles, bulk sensitivities tend to range between 100 and 500 *nm/RIU*. These values can significantly increase for more complex structures [104], such as bipyramids (540 nm/RIU), nanoprisms (583 nm/RIU) [59], ring-disk nanocavities (648 nm/RIU) [105] or nanocrosses (1000 nm/RIU) [106]. Either way, the lack of information of their surface sensing performance is not that surprising, especially when taking into account the work carried out by Piliarik *et al.*, in which a gold nanorod is used as an example to illustrate the strong correlation that exists between the surface sensing performance and the EM field profile of the LSPR [107]. From this work it can be concluded that for a good assessment of the surface sensing capability of a nanostructure, it becomes necessary to assure a homogeneous coverage of the nanoparticle´s surface with biomolecules, or, even

more important, to channel molecule binding uniquely to those regions of the particle that exhibit the highest sensitivity. This latter approach becomes especially desirable to enhance the surface sensitivity but simultaneously is really difficult from an experimental point of view, especially when considering that nanoparticle surface chemistry still lags behind thin film surface modification protocols. As a conclusion, we can point out that in order to fully exploit the biosensing potential of more complex nanostructures, the functionalization on the so-called EM hotspots of the structure, typically being sharp edges, or small cavities, should become the main challenge to be surpassed.

3.2.2. Sensitivity Improvements

As briefly introduced in the previous section, two aspects that turn out to be especially relevant when trying to maximize the biosensing performance of nanoplasmonic sensors are: (i) the directed biofunctionalization of the metallic nanostructures leaving the supporting substrate unaltered and (ii) overcoming intrinsic negative influences that the substrate itself (typically glass/silicon-based materials) can have on the sensing performance.

Directed Functionalization

The field that offers most margin for the improvement of the LSPR sensing performance is related to the proper surface functionalization of the plasmonic nanostructures, that is, *directed functionalization*. However, this aspect is often under-highlighted in published studies of refractometric LSPR biosensing. Before going into further detail, it must be mentioned that the functionalization process for SPR sensors is much more simplified: whereas in thin film sensing biomolecules *see* a homogeneous gold surface at which binding can take place, in LSPR sensors part of the underlying substrate is typically exposed, making undesired non-specific binding events to this substrate easy to occur. In this latter case, ideally all molecules reaching the nanostructured surface should be anchored solely to the nanostructures, and preferably, only to those places that find themselves in the vicinity of EM hotspots, where RI sensitivity

415 is maximized. However, only few examples exist in literature that proactively attack this problem. Most
416 probably, inherent complexities related to accurate orthogonal modification of both materials lie at the
417 heart of the problem: in an ideal system one would functionalize the metallic nanostructures with the
418 biomolecules at a given desired surface density concentration, while the underlying substrate is blocked
419 with materials or compounds that assure its inertness to both the immobilized biomolecules and its
420 corresponding target. A study that exemplifies this very well was carried out by Feuz *et al.* [108]. In this
421 work, thin gold nanohole films fabricated on top of a TiO_2 substrate are used in combination with a
422 proof-of-concept protein sensing assay (detection of Neutravidin by biotinylated surfaces), to provide a
423 comparable study that demonstrates that by assuring both previously mentioned demands, the LOD of
424 this particular system can be extremely improved, offering an approach that can be extrapolated to
425 other nanoplasmonic sensing platforms. By only exposing the highly sensitive inner walls of the
426 nanoholes to the surrounding dielectric, the authors assure the binding of molecules to the most
427 sensitive regions of the transducer surface (see Figure 4.A.). Furthermore, a material-selective
428 poly(ethylene glycol)-based surface chemistry limits the binding of NeutrAvidin only to surface
429 immobilized biotin that finds itself on the exposed gold regions. By doing this, a 20-fold enhancement of
430 the sensor response time is reported. It should be noted that the controlled immobilization onto the
431 gold areas with highest sensitivities is not achieved by surface chemistry but by the nanostructure
432 fabrication process itself. The latter is done by sandwiching the gold nanohole substrate between two
433 TiO_2-layers. This strategy clearly simplifies the chemistry and reduces the complexity to discriminate
434 between TiO_2 and gold. In an alternative, but conceptually similar methodology, the same authors have
435 developed a more complex material-selective surface chemistry protocol [109]. In this case, gold
436 nanodisk dimers were fabricated on SiO_2 substrates using bioactive TiO_2 layers located in the gaps
437 between the gold disks (see Figure 4.B.). By appropriately choosing pegylated compounds that
438 selectively react with Au, TiO_2 or SiO_2, biomolecules could be immobilized exclusively in these high EM-

field gaps, assuring enhanced sensitivities. When comparing this sensitivity to the case where the molecules are uniquely bound to the gold nanodisks, a four-fold larger signal per bound molecule was obtained (Figure 4.B.).

Another interesting strategy takes advantage of thiol place-exchange processes. Using gold nanoplates grown on glass or silicon surfaces, Beeram *et al.*[110, 111], followed this procedure by first covering the surface with a non-reactive thiol. Then, subsequent addition of another thiol-modified compound (in this case incorporating a reactive carboxylic group) induces an exchange process of reagents, occurring preferentially at edge- or vertex sites of the nanostructures (which turn out to be approximately 2-3 times more sensitive than terrace sites) (see Figure 4.C). Following this path, the binding of antibodies (anti-IgG) exhibited a higher sensitivity compared to the case in which the nanoplates were entirely covered with the reactive thiol group. Moreover, the detection of target IgG resulted in a LOD 500 times lower than the one obtained with conventional antibody coverage of the nanoplates, even using much higher concentrations of anti-IgG receptor molecules (10x). Also, the length of the thiol linkers, used to control the distance from the surface, have a significant effect since larger spectral shifts are obtained for short thiols [111].

Substrate Effects

The required attachment of lithographically fabricated nanostructures to underlying substrates imposes significant intrinsic drawbacks on the sensing performance of LSPR sensors. To assure a robust binding of the nanostructures, often, extremely thin metal adhesion layers are employed to form a bridge between the plasmonic material and the substrate. However, the use of these metal adhesion layers increases the LSPR dephasing time, reducing the scattering amplitude and inducing peak broadening. Judging from a biosensing point of view, this aggravates the signal to noise ratio of LSPR sensors, resulting in inferior sensing performances. Therefore, a proper choice of material and geometry has

462 proven to be of critical importance to provide competitive sensor performances [112, 113]. In thisline,
463 plasmonic resonances can be improved by replacing the metal adhesion layer by a thin molecular layer
464 (i.e. (3-mercaptopropyl)trimethoxysilane) which binds both the glass substrate (through the silane
465 group) and the metal (through the thiol group)[114].

466 Furthermore, the supporting substrates (typically glass) possess a RI that is much higher than those
467 corresponding to the buffer solutions normally used in bioassays. As a consequence, the symmetry of
468 the EM around the nanostructures is broken, shifting a much larger part of this EM field towards the
469 metal/glass interface. Here, this EM field is almost entirely insensitive to RI changes of the external
470 dielectric medium, significantly lowering the overall sensitivity of the nanoplasmonic structures [115]. To
471 overcome this problem and improve the sensing features of the nanostructures, the effective RI
472 surrounding the nanostructures has to be decreased. The use of low RI materials as supporting
473 substrates presents itself as a very straightforward method to overcome this problem. Following this
474 route, *Brian et al.* showed that a Teflon (n=1.32) substrate supporting a thin gold film perforated with
475 nanoholes yielded a 40 % improvement of the bulk sensitivity [116]. Another strategy relies on placing
476 the nanostructures on nanopillars, distancing them with respect to the underlying glass substrate. These
477 dielectric pillars can be created *during* the lithographical fabrication process [117, 118], or *afterwards*,
478 using an isotropic etch of the glass substrates (see Figure 5). Following this path, all the hotspots of the
479 nanostructures are exposed to the surrounding dielectric, increasing the particle surface available for
480 biosensing, leading to sensitivities that are comparable to that of *free* nanostructures in a homogeneous
481 dielectric medium [112]. The latter was achieved via DNA hybridization measurements.

482 3.3 LSPR Biosensing: Applications and Issues

483 The previous sections have highlighted fundamental aspects that researchers are implementing to
484 improve the performance and the capabilities of nanoplasmonic biosensors. However, its transfer to

485 real applications is not that straightforward. When aiming at the detection of low amounts of molecules
486 and pushing high throughput capabilities to the limit, single particle sensing is the preferred option.
487 Currently, array-based LSPR biosensors are most commonly used. Some results reported in the literature
488 using array-based nanostructures in which their sensing performance is directly compared to
489 conventional SPR sensing, seem to be encouraging, while simultaneously, other publications reveal
490 aspects of refractometric LSPR sensing that inevitably generate serious doubts about its real potential.
491 For instance, Homola's group developed a high-resolution LSPR setup and did some experiments on
492 ordered nanorod arrays determining their surface coverage with DNA sequences. They concluded that
493 although LSPR-based biosensors can detect a number of molecules (i.e. number of interactions) two
494 orders of magnitude lower than SPR-based sensors, which is clearly advantageous, the resulting
495 analytical performance is very similar compared to other high-resolution SPR setups [119]. This result is
496 most probably due to the kinetics of the interaction as the probability of the biomolecular interaction is
497 also proportional to the number of interacting molecules. Linked to this result, and putting more focus
498 on the influence of the fluidics and the kinetics of the reaction, a recent study by Sipova *et al.* [120]
499 compared the performance of SPR and LSPR-like sensors to detect interactions events in flow-through
500 formats. The study was done by comparing a flat surface covered with receptors, resembling an SPR
501 system, with a situation in which a single receptor is immobilized on the surface, for the detection of
502 single binding events, being approximately analogous to an LSPR-like system. The estimation concluded
503 that for common biomolecular interactions (antigen-antibody, DNA-DNA, etc.) and for typical detection
504 times (10 min) the probability of positive response, that is, of detecting a single molecular interaction in
505 the case of a single receptor (i.e. in a single nanostructure) is much lower (between 10 and 10^3)
506 compared with flat surfaces homogeneously covered with receptors. The reason behind this is precisely
507 due to the low number of recognition elements available in LSPR sensing and only seems to approach
508 SPR performance when dissociation rates are extremely high and/or when the analytes are small.

Although for static end-point analyses these conclusions may not be the same, these results exemplify the existing debate about the real necessity of pushing forward single event detection with nanoplasmonic platforms as next-generation biosensors from a strictly practical analytical point of view. In the following we discuss some recently reported relevant works that include both the use of single nanoparticles and array-based nanostructures as sensing platforms for real biosensing experiments.

3.3.1 Single Particle Sensing

The detection of discrete binding events with single nanostructures has positioned itself as the ultimate goal for future biosensors which share high throughput capabilities, low sample consumption and extremely low limits of detection among their main characteristics. However, from a strict biosensing perspective, where detecting low concentrations of target is the main goal, the potential and feasibility of label-free single particle sensing is probably more limited. Whereas the spectral readout setup can be easily adapted to single particle detection using microscopy, there are still some general issues related to poor signal-to-noise ratios. Although this can be significantly improved by implementing near-normal incidence DF microscopy instead of more conventional large incidence angle schemes [121], DF microscopy generally provides low signal levels and insufficient time resolution for the detection of few/single analytes. Also, it usually results in fair sensitivities and long-time analysis [122], caused by mass transport limitations [123, 124]. Recently, by expanding a conventional DF microscopy scheme with a broadband laser source and an intensified CCD camera, Ament *et al.* demonstrated the label-free single protein detection with an individual metallic nanostructure [125]. Contrary to prior work, their technique offers impressive levels of time-resolution (ms time scale, with between 4 and 6 orders of magnitude better levels than previous reported works) and measurement noise (tens of pm). Furthermore, Zijlstra *et al.* demonstrated that the detection of individual target analytes can also be achieved by making use of photothermal microscopy [126]. Gold nanorods - biotinylated mainly at the tips [127] - were immobilized on the surface and three biotin-binding proteins with different molecular

weight were discretely detected, observing step-like signal-enhancements proportional to their sizes [126]. Also, in order to allow for multiplexed spectral interrogation of single nanoparticles, much effort is being put in devising techniques for parallel read-outs. We can distinguish techniques based on the use of conventional DF microscopy, in which the spectral readout is either carried out with the use of a liquid crystal tunable crystal [128], gratings [129], or advanced image processing algorithms [130] for the parallel spectral read-out of multiple nanostructures. The latter approach is especially interesting, since next to parallel read-out, this methodology normalizes the LSPR of geometrically different nanoparticles. This minimizes the influence of inherent differences in the same batch of nanostructures, avoiding the necessity of averaging several nanoparticles while improving fitting parameters in biosensing assays. But despite the benefits of these methods, a great challenge lies ahead in order to provide these techniques with improved signal levels, and hence, better time resolution, to make them really useful to study the real-time kinetics of surface binding events.

In terms of applications, a variety of recent examples have appeared in literature. Until recently, single molecule/event detection has been restricted to the use of labels, due to the limited resolution of peak shift resolution in most common LSPR-based technologies. Amplification schemes based on the use of gold nanoparticles, which monitor single DNA hybridization events [131] have been reported. Another approach is based on exploiting the catalytic activity of the enzyme Horseradish Peroxidase (HRP), which in this proof-of-concept study was used as target itself [132]. Exploiting the catalytic activity, few or even one HRP molecule can be detected on conical nanoparticles, by adding a substrate which produces a precipitated product. The binding of the enzyme on the surface of the nanostructures induced the localization of the precipitate on the very same structure, significantly enhancing the overall signal, and improving the detectability. The strategy could be adapted to detect other type of molecules which incorporated HRP as labels in an ELISA-like assay, which inevitably prevents a label-free approach. On the other hand, strict label-free single-particle sensing has already been attempted to evaluate self-

557 assembled monolayer formation, in this case, on silver nanoparticles [133] and also for proof-of-concept
558 biotin-streptavidin detection either with nanoparticles [58, 134, 135] or nanoholes [136].

559 Some examples of protein detection by immobilizing aptamers or antibodies on nanoparticle surface
560 (either nanospheres [130, 137] or nanorods [138, 139]) have also been reported, showing its potential.
561 In some cases, sensitivities in the attomolar range are achieved [138], although it should be mentioned
562 that this involved end-point measurements. Huang *et al.* [140] have detected TNFα protein using
563 immobilized Ag nanoparticles (2.6 nm) functionalized with its specific antibody using DF single
564 nanoparticle optical microscopy and spectroscopy (SNOMS). Although acquisition times of several hours
565 were necessary, the high sensitivity of these small-size NPs assured single molecule detection and the
566 study of the binding kinetics. Song *et al.* [141] employed single particle sensing to study DNA-protein
567 interaction, in particular, to estimate the relative promoter activity, by immobilizing the DNA sequence
568 (SP6 promoter and single point mutation variants) and detect promoter Polymerases (SP6 RNA
569 polymerase). What adds special interest to this work is that, contrary to conventional methodologies,
570 real-time kinetics of the reaction was studied. Mayer *et al.* demonstrated the detection of single
571 capturing and unbinding events using single gold bipyramids in real time, paying special attention to the
572 dissociation rather than to the binding events, since it is slow enough to detect it in the time resolution
573 frame, and should not be affected by initial concentration or diffusion effects [53]. The relatively long
574 timescale of the process (10^5 s) turns out to be an advantage to detect single events. This approach can
575 provide valuable fundamental information regarding nanostructure behavior and protein interaction
576 dynamics in comparison with labeled methodologies such as FRET (fluorescence energy transfer
577 processes) [142], which require modification of molecules and limits time scale to the stability of the dye
578 used, being sometimes short to some purposes (i.e. 10^2 s).

3.3.2 Particle Array Sensing

As previously discussed, whereas single particle sensing offers outstanding potential from a multiplexing point of view, and avoids inherent "signal-averaging effects" when dealing with nanostructured surfaces, this concept exhibits some important drawbacks which prevents its extensive use for routine biosensing analysis. In this regard, biosensing schemes based on arrays of nanostructures not only offer improved possibilities for cheap and mass-scale chip production, but also hold the advantage of keeping the required instrumentation very simple. It comes therefore as no surprise that most nanoplasmonic biosensing studies currently rely on the use of nanostructured substrates. As is also the case for single particle sensing, besides some relevant examples published some years ago[143, 144], the majority of recent publications keeps being limited to a proof-of-concept based on a routine biomolecule immobilization and subsequent target detection. More in-depth analyticalstudy, including a complete optimization of the bioassay to set its reproducibility, sensitivity, specificity and viability to detect targets in complex samples is yet rare to find. Besides, often end-point analyses are carried out instead of real-time measurements that monitor the reaction kinetics. Even more, end-point measurements are generally carried out in air after performing successive incubation/washing steps, thereby inevitably affecting their reproducibility and increasing measurement times. On the contrary, in the case of real-time monitoring, the use of a fluidic cell prevents the samples from drying, ensuring that biomolecules remain under favorable aqueous environment which minimizes their denaturation and also facilitates the kinetics analysis [145]. The most recent works, which are characterized by a proactive strategy that addresses one or more of these previously mentioned aspects are discussed in the remainder of this section and summarized in Table 1.

When considering nanostructured arrays, one can initially distinguish between particle- and hole-based nanostructures, being the particle based one the more extensively used for nanoplasmonic biosensing. Most of publications employ antibody-based strategies, either for the detection of proteins or viruses,

603 DNA interactions or with more unusual approaches such as the study of supported lipid bilayer
604 formations. Among them, some stand out for handling interesting issues related to biosensing. For
605 instance, although no in-depth optimization has been performed, Zhou *et al.* used an integrated LSPR
606 sensor based on Ag nanotriangles fabricated by NSL to detect p53 protein levels in serum from cancer
607 patients (patients with head and neck squamous cell carcinoma, HNSCC), which is commonly
608 overexpressed when compared to healthy patients. Specific antibody against p53 was covalently bound
609 to the nanoparticle surface, and detection was done with incubation steps and static measurements.
610 Unfortunately, no protocol optimization, reproducibility estimations or studies related to the influence
611 of serum were presented. Similarly, but including real-time dynamics analysis, Chen *et al.* [146],
612 demonstrated the detection of two different proteins (PSA and Extracellular adherence protein EAP)
613 using specific antibodies immobilized on the surface of gold nanodisks. In this case, estimated LODs
614 ranging between 1-8 pM were reported (compliant with the requirements for clinical applications).
615 However, also in this case, neither specificity studies nor detailed assay optimization were addressed.

616 More in-depth biosensing analyses have been reported using Au-capped nanoparticles [147], fabricated
617 using a dense monolayer of silica nanoparticles on top of a gold substrate as a core template for the
618 subsequent deposition of a thin Au film (tens of nm). Their ease of fabrication, strong LSPR and
619 integration in simple optical setups yields very compact nanoplasmonic biosensing schemes which are
620 typically based on static absorbance measurements done after intermediate incubation steps. Despite
621 the fact that no cell- or microfluidics are employed, the assay optimization and the reproducibility
622 studies confirm the robustness of the approach. This type of substrate has been exploited for a variety
623 of biosensing applications, most of them with a clinically relevant goal, either using antibodies or nucleic
624 acids as active recognition elements. A selection of successful results are gathered in Table 1, where one
625 can highlight for instance the detection of proteins in complex media (detection of casein protein in milk
626 with antibodies immobilized on the surface using Protein A as orienting molecule [147]). Another

remarkable example is based on the detection of cell activity and cell function (i.e. determination of cell metabolites such as Interleukin-2, IL-2). This is achieved by immobilizing specific antibodies against these metabolites. Afterwards the cells are simply deposited and appropriately stimulated in order to trigger the metabolism to produce and secrete certain molecules which can be captured by the antibody [148]). Other biosensing examples are focused on the detection of relevant biomarkers for Alzheimer's disease using specific antibodies [149], the interaction of toxins with membranes which are immobilized on the surface [150] or fibrinogen detection, mediated by antibodies which are immobilized in an oriented manner using a specific aptamer that recognizes the Fc (constant fraction) of the immunoglobulin [151].

Multiplexed analyses can be implemented through the use of biodeposition systems [152] or by adapting the fabrication to obtain multiple areas of gold-capped nanoparticles, (multispot gold-capped nanoparticle arrays, MG-NPA) which can be individually immobilized and interrogated (i.e. between 15-60 spots and sizes in the mm range), assuring higher levels of throughput. This approach allowed for the detection of antigens related to the hepatitis B virus [153], the detection of antibodies recognizing influenza virus [154] or the detection of DNA point mutations related with corneal dystrophies [155], which was validated with real patients' samples. Furthermore, Cu-capped nanostructures have been used to carry out a complete multiplexed biosensing experiment in which pathogenic bacteria DNA was directly detected in real isolates coming from samples as blood, pus, urine or sputum exhibiting sensitivities in the fM range [156].

Recently, alternative biosensing approaches based on specific recognition events have been reported that offer interesting results beyond clinical diagnosis. For instance, using self-assembled gold nanorods, the detection of chiral compounds has been showed using enantioselective sensitive receptors [67], being a good example of LSPR sensing in the field of drug-protein interactions. In this work, the nanostructures, immobilized on the inner walls of a microfluidic channel, were functionalized with

650 human α-thrombin that was used as the selective receptor. Then, a complete optimization of the
651 protocol for the detection of the drug *RS*-melagatran was performed, achieving discrimination of the
652 enantiomeric counterpart (*SR*-melagatran). Besides, although at the cost of a diminished sensitivity, the
653 target could also be detected in human serum. This concept has been further expanded for the
654 discrimination of a racemic mixture (in this case for (*R*) and (*S*)- 1,2,3,4,-Tetrahydro-1-naphtylamine,
655 TNA), using weak or non-enantioselective receptors instead of strong ones. In this case, the authors
656 used a dual channel microfluidic chip, with a weak chiral receptor in one channel and a nonselective
657 receptor in the other one [157]. By combining the information extracted from both channels it was
658 possible to determine the individual concentration of each enantiomer of TNA in a racemic mixture.

659 Another biosensing concept that has been recently exploited involves the detection of conformational
660 changes in proteins, which is more plausible to be detected using the strong EM field confinement of
661 LSPRs than with the more deeply penetrating evanescent fields of conventional SPRs. In this case the
662 focus does not lie on the direct detection and quantification of a specific target, but on the study of the
663 protein structure or interactions against external stimuli or interactions with small molecules, which,
664 due to their low molecular weight, would otherwise be difficult to detect by simply binding them to the
665 surface. This is the case recently reported by Hall *et al.* [158], where Ca^{2+} was detected in a label-free
666 manner, by monitoring the conformational changes of the protein calmodulin immobilized on the
667 surface of Ag nanoprisms. The changes in the conformation affect the density and overall height of the
668 protein immobilized layer, resulting in spectral LSPR shifts. A low-noise level (0.002 nm and S/N levels of
669 500), together with a well-controlled immobilization of calmodulin, which ensures the proper
670 orientation of the globular domains responsible for the interaction with the ion, resulted in Ca^{2+}
671 detection at concentrations as low as 23 μM. Furthermore, the strong EM field confinement of LSPRs,
672 which can be exploited to increase the sensitivity to detect small molecules, can be further enhanced by
673 taking advantage of another phenomena, derived from the strong coupling between molecular

674 resonances of chromophores and the LSPR, resulting in larger spectral shifts [159]. This has been used to
675 study the interaction of small drugs with human membrane-bound cytochrome P450 3A4 (CYP3A4),
676 which contains a heme chromophore group [160]. In this work, CYP3A4 was first stabilized in the form of
677 soluble nanodisks with membrane scaffold proteins, and then immobilized onto Ag nanoparticles. The
678 binding of a variety of small drugs (MW~ 100-700 Da) has been tested and the observed spectral shift
679 (blue shift, red shift or no shift) identifies different interaction types.

680 Whereas particle arrays are solely dominated by the LSPR of the nanostructures, nanohole substrates
681 present additional peculiarities due the co-existence of surface plasmons that propagate along the metal
682 film and localized plasmons excited inside individual nanoholes, whose interaction can give rise to
683 exciting optical phenomena such as Extraordinary Optical transmission (EOT) [161] or interacting anti-
684 symmetric plasmons [162]. Over the years, nanohole substrates have been extensively studied, both
685 from a fundamental and practical point of view. Since the spectral interrogation of nanohole films relies
686 on simple transmission measurements, thereby lacking the need of prism-coupling, and hence,
687 noticeably simplifying the optical measurement schemes [163, 164], their use for biosensing has been
688 widely suggested [165-169]. Similarly to particle-array this particular measuring scheme is also
689 compatible with imaging configurations [3], opening up facile routes towards multiplexed sensing
690 assays, as demonstrated in some biosensing applications, including quantification of ovarian cancer
691 biomarkers with an integrated microfluidic platform[170], studies of antibody-ligand binding kinetics
692 [166] or simultaneous detection of antibody-target binding events in temperature regulated flow cells in
693 microarrays based substrates [171]. However, these measurements generally tend to exhibit moderate
694 sensitivities, even lower than SPR-based biosensors, as demonstrated in these previous examples (in the
695 nM range [166, 170]. Better sensing performances for high throughput measurements can be achieved
696 introducing dual-color filter imaging [90], resulting not only in better sensitivities, but also in increased
697 accuracy and signal-to-noise ratios. On the other hand, when studied in a conventional Kretschmann

configuration it turns out that these nanohole array films exhibit enhanced bulk sensitivities compared to planar gold surfaces. These sensitivity enhancements can be precisely tuned using the periodicity of the holes and their geometry as variables [172], although resulting in lower resolutions [173]. Besides this enhancement of sensitivity on thin gold film, strong localized plasmons are generated in the hole [174-176], providing an enhanced sensitivity in these areas. Due to the coexistence of propagating and localized excitations at the same time, the behavior of these LSPRs is quite complex being the shape and size of the hole, the lattice periodicity and the substrate material important parameters governing both phenomena [116, 167, 177]. Biosensing schemes that exploit the LSPRs excited in the nanohole itself possess the attractive advantage of minimizing the required sample volumes, as long as accurate immobilization in these areas occurs. The resulting reduction of the sensing area will eventually proclaim better sensitivities, opening up pathways towards very low LODs [163]. Besides the biosensing examples described above, other relevant applications have been based on the formation of supported lipid bilayer (SLB) formation. The addition of a silicon-based layer over nanohole structures permits the formation of SLB and has allowed studies that involve cell membrane related biorecognition reactions [178, 179]. Besides, SLBs have been used as myelin-mimicking bilayers to kinetically characterize autoantibodies involved in neurological disorders [180]. Nevertheless, as of today, the advancements made in the fabrication of these nanoholes structures and the reported studies that discern their optical features have not been fully transferred to a routinely used biosensing scheme and the majority of the examples in the literature do not surpass the proof-of-concept level in which a simple biofunctionalization of the surface followed by a preliminary detection assay is carried out, thereby fully neglecting any further optimization of the addressed biosensing assay.

Currently, one of the most promising uses of nanohole arrays for the creation of refractometric nanoplasmonic sensors relies on suspending these structures, such that the holes act as nanochannel-based structures. In this configuration, the analytes are forced to flow through the nanometer-sized

sensing channels, where the nanohole concentrates the most sensitive areas. This approach does not only enhance the analyte delivery, but also improves the binding efficiency and reduces the sample consumption. Gordon's group [181-183] demonstrated the applicability of these structures as optofluidic sensors achieving a significant enhancement in adsorption kinetics compared with flow-over strategies and a 2-fold LOD improvement by concentrating the target in the nanohole proximity [184]. Biosensing was demonstrated as proof-of-concept by binding an antibody to a previously functionalized surface. Real time measurements can be performed due to the introduction of a fluidic cell integrating the sensing structure. Altug's group designed a very similar structure with a bulk sensitivity of 535 nm/RIU [185]. Furthermore, a 14-fold improvement in the mass transport rate constants was achieved [186]. Virus detection based on the immobilization of specific antibodies onto the surface (not restricted to the in-hole section but over all the metal surface) has been demonstrated with this design, although the measurements were based on end-point analyses, requiring long-time incubations (60-90 min) and no microfluidics were used [187]. Hook *et al.* have also fabricated so-called nanopores based on suspended arrays of nanoholes [188]. However, besides the optimization of the structure and its characterization, these authors have devoted a great effort in the controlled functionalization of gold areas while protecting the rest of the substrate (SiN) from non-specific adsorptions: the use of appropriate antifouling compounds such as pegylated compounds with thiols or with poly-lysines, allow the particular binding to each region (gold or silicon, respectively), thereby minimizing nonspecific adsorptions. If the thiol-pegylated compounds also contain additional functionality (i.e. biotin groups), subsequent biofunctionalization can take place and can be controlled at the areas of interest (gold and not silicon). These experiments showed a 10-fold faster response as compared with non-suspended holes with diffusion-controlled binding.

3.4 Integration, Microfluidics and Multiplexing

Despite the reported advantages of LSPR-based sensors in terms of multiplexing and integration, only few works have dealt with these aspects. So far, to our knowledge, only one product has reached commercial implementation [189]. Lamdagen Corporation has launched a device based on LSPR for laboratory use. The device allows real time measurements using syringe pumps and nanostructured metallic films as sensing chips. Four or eight-spot arrayed substrates can be used which can be simultaneously monitored, yielding a medium degree of throughput. The device consists of light sources connected to optical fibers to direct the light onto the surface and output optical fibers which collect the reflected light directly to individual spectrometers, permitting individual channel monitoring. The equipment also incorporates software to analyze the data. The reproducibility and robustness of the system seems to be high and complex media such as serum and saliva can be analyzed. Despite this potential, the sensitivity levels in a label-free configuration without the aid of amplification are still fair, lying in the nM range. Nevertheless, this is an interesting example of integration LSPR system, and can be considered an initial step towards point-of-care devices.

Nanoplasmonic point-of-care devices inevitably require three crucial aspects: compactness, ease-of-use and potential for high-throughput. Removing the need of a spectrophotometer and using light emitting diodes (LEDs) as LSPR excitation source can specifically contribute to simplification of the system, as recently demonstrated by Huang *et al*. [190]. The authors have designed a setup where a LED (λ=530 nm) is used for plasmon excitation, while a quadrant photodetector is used to continuously measure the change of the transmitted light at a fixed wavelength (see Figure 6.A.). Dual-channel microfluidics (for sample and reference) has been fabricated and integrated with the nanoplasmonic chip. This flow cell incorporates an automated sample delivery system consisting of an off-chip micropump and microvalves [191]. Calibration curves of the interaction of Anti-biotin antibody to biotin-coated nanoparticle surface

767 were demonstrated as proof-of-concept, although with limited sensitivity, mainly due to the properties
768 of the substrate (gold nanoparticles that rendered a sensitivity of 10^{-4} RIU and a LOD of 270 ng/mL of
769 antibody).

770 A similar approach was presented by Neuzil *et al.* [192], in which a palm-size reflectance-based LSPR
771 sensing scheme was fabricated, that also uses LED illumination and a photodiode-based detection
772 scheme, yielding a simplified setup (see Figure 6.C.). In this case, instead of a single LED, four different
773 LEDs were combined, to improve either data normalization or to simply allow for a more efficient
774 selection of the most suitable one for a specific application. The reflected light coming from each LED is
775 lead to a single photocurrent output, after which the signals are de-multiplexed and digitized, before
776 being displayed on an incorporated LCD display. Although the device undoubtedly shows good potential
777 for future point-of-care devices, the lack of incorporated microfluidics forces the measurements to be
778 based on static incubation. However, up to this moment, no biosensing demonstration of this device has
779 been presented.

780 More recently, another portable transmission-based nanoplasmonic sensor has been reported [193],
781 based on the use of three individual LEDs combined with on-board signal amplification (Figure 6.B). This
782 scheme uses the monitorization of spectral LSPR shifts, using an algorithm that extracts the spectral
783 position of the resonance both before and after molecular interaction events. Immobilization of single-
784 stranded DNA was carried out as a proof-of-concept. However, the straightforward subsequent
785 detection of complementary target has not been yet tested, and moreover, the measurements were
786 performed in air under static conditions. Also aiming at increasing the compactness of the sensing
787 devices, Mazzota *et al.* [194] have presented an integrated detection based on the use an array of small
788 photoactive diode regions (i.e. silicon p/n junctions) that act as independent photodetectors. In this
789 case, two of them have a nanostructure patterned on their surface (nanodisks on Si_3N_4 coated glass),

while the other two are used as references. Changes in the extinction spectra caused by binding interactions then result in real-time measurable changes of the photocurrent output. By incorporating the nanoplasmonic chip in a flow cell, its biosensing capability was shown by preparing a biotinylated surface and subsequently monitoring the real-time binding of Neutravidin. Furthermore, also implementation of a Vertical-cavity surface-emitting laser (VCSEL)- optical excitation, combined with a CCD camera for detection, significantly reduces the dimensions of the setup [195]. In this work, the biosensing measurements based on the study of biotin-neutravidin interactions, showed similar outcome when compared to the use of a spectrophotometer.

The advantage of using a CCD camera for multiplexed measurements with an LSPR-based device has recently been demonstrated by Ruemmele *et al.* [196]. They have reported the first example of full spectral imaging of a macroscale LSPR sensor array by modifying and adapting a commercial SPRi with a liquid crystal tunable filter (LCTF), a flow cell and by aligning the camera with the illumination path (See Figure 6.C.). The LCTF, which is used to filter the white light illuminating the nanoplasmonic chip, enables the monitorization of either visible or near-IR wavelengths. While scanning, a camera simultaneously captures images whose intensity maps are then correlated with wavelength, enabling the extraction of region-specific LSPR spectra, whose spatial resolution is theoretically diffraction-limited. Substrates with sizes of 6.45 cm^2 containing different nanodisks areas, which can be individually biofunctionalized and monitored were fabricated. Simultaneous binding measurements could be performed over an area of around 1.1 cm^2 and as proof-of-concept two approaches were demonstrated: (i) homogeneous coverage of the nanodisk surface with biotin at a unique concentration and anti-biotin detection at different concentrations, using static measurements whose results yielded a calibration binding curve; (ii) the controlled immobilization at different areas using different DNA probe concentrations and a subsequent in-flow delivery of the complementary sequence at a single concentration; in this case, multiplexing throughput is incorporated under dynamic conditions. Although

not compact enough to be denominated as “lab-on-chip”, this is an attractive approach that attempts to expand LSPR sensing with multiplexed capabilities, similar to the transition of SPR to SPRi.

The previous examples aim at the integration of the optical components and those needed for the different detection read-outs; in this regard, some of them use static measurements while others allow for in-flow sample injection via the use of custom-made single-channel flow cells.

However, the successful implementation of more complex microfluidics, that assure both miniaturization and improved throughput capabilities, still remains a challenging task. In literature some examples can be found of nanoplasmonic biosensing with more elaborated PDMS microfluidics, ranging from a few fluidic channels, (1-2 channels [197, 198]) to high throughput chips (nanohole substrate with 50 channels monitored in parallel by a CCD camera [199]). Next to PDMS, other polymeric materials offer more compatibility with mass production and low-cost fabrication such as cyclic olefin copolymer (COC). COC has profiled itself as an interesting alternative material for the fabrication of microfluidic systems, illustrated by the previously described dual-channel system designed by Huang *et al*. [190]. A more complex configuration that incorporates up to 64 differentiated incubation chambers is described by Malic *et al.* [200]. They have designed and fabricated monolithic thermoplastic microfluidics which is based on three layers: the nanostructured bottom layer (flow layer), which, next to the chambers (8x8) and the fluidic channels, also incorporates the plasmonic nanostructures (nanogratings); the top layer (control layer) which is built out of a thermoplasmic elastomer (TPE) and allows the integration of reservoirs and active fluidic elements such as an array of pneumatic valves to ensure the delivery of fluids; finally, an intermediate membrane whose main function is the assembly of the entire device. This apparatus operates under pressure driven flow supplied by a multichannel syringe pump equipped with switching valves for sample loading. The design allows both differentiated functionalization and detection in a row/column configuration. This is done by opening/closing the corresponding valves of

each functionalization/sample loading channel in such a way that up to 64 different conditions can be tested. The experimental setup is designed to perform sequential transmission measurements, by using a XYZ rotational stage to individually align the illumination source with each chamber. The authors have characterized the device in terms of bulk sensitivity and more interestingly, they have done kinetic real time measurements for the detection of CD44, a clinically relevant biomarker. They have monitored all the steps, from the surface derivatization with a thiol-based reagent, to the attachment of specific antibody anti–CD44 and the subsequent detection of CD44 at different concentrations, enabling the determination of binding and affinity constants. Direct detection (with a LOD of 5.26 nM) and also amplification with a secondary antibody to improve sensitivity (up to a LOD of 10.53 pM) were performed, with reproducibility studies included. This impressive high-throughput approach would gain additional merit, especially when viewed from a POC perspective, if parallel read-out of all chambers could be performed.

4. Considerations, Future Trends and Conclusions

As reflected in this review, the work published in the field of refractometric nanoplasmonic biosensing is often of a very fundamental nature. Without a doubt, the main reason behind this is the relative youth of this ever-expanding field of research. Examples in literature of nanoplasmonic sensing schemes that report interesting biosensing capabilities are typically accompanied by novel nanoplasmonic structures that often rely on new material properties. In most cases, the novelty of these *new* materials relegates their use as biosensing platforms to a secondary plane. In this regard, these studies are often accompanied by – far from optimized – preliminary proof-of-concept biosensing assays.

Several of these works clearly illustrate the great potential offered by nanoplasmonic structures as biosensing platforms. On this subject, one should emphasize several - previously discussed - studies at a single particle level that attribute better sensing performances to specific nanoparticle geometries, such

as nanorods, when compared to conventional SPR sensors. The most eye-catching example is undoubtedly the successful accomplishment of single-molecule detection, often considered the most important milestone of nanoplasmonic sensing. However, the voluminous and expensive experimental setups needed for the spectral interrogation of single nanoparticles, infringes the demands required for the creation of compact and low-cost platforms that can be used out of the laboratory.

To achieve the latter, more opportunities are offered by sensing schemes based on nanostructured substrates, which, accompanied by facile experimental setups, possess much more opportunities for the fabrication of compact and integrated devices, with real possibilities of technological transfer into commercial products. However, on the downside, the reported biosensing performances of nanoplasmonic sensors based on this concept are typically of the same order as standard SPR sensors [97], thereby not adding any significant benefits when it comes to sensing performance. Although this can be compensated by other interesting properties, like miniaturization, integration and multiplexing capabilities, the sensitivity typically is considered the key factor that makes or breaks the potential of a sensing scheme.

During the last lustrum, an ever increasing scientific interest can be observed involving the use of plasmonic metamaterials for sensing purposes. These metamaterials, consisting of precisely tailored nanostructured substrates that exhibit optical properties not seen in nature, can give rise to exciting optical responses with high FOM-values, suggesting their potential use as nanoplasmonic sensing platforms. In this category, a special interest goes out to Fano resonances, that is, optical modes caused by interference of continuum broad optical modes and strong localized plasmons. The optical modes are excited in precisely engineered or even self-assembled nanostructures [201], and exhibit either sub- or super-radiant optical modes with asymmetric and sharp spectral fingerprints [202], making a strong argument for their employment as refractometric biosensing schemes [105, 106, 203-209]. Also,

883 metamaterials based on ordered arrays of nanoparticles, which support a guided mode which can be
884 caused either by near-field interactions or diffractive far-field effects, have appeared to be interesting
885 for refractometric sensing applications [88, 89, 210-213]. Furthermore, also arrays of randomly ordered
886 gold nanodisks have been shown to act as thin layers of meta-atoms with very high effective RI, allowing
887 the guidance of in-plane EM modes [214]. Through the use of these guided modes, the overall
888 biosensing performance of isolated gold nanodisks can be improved by more than one order of
889 magnitude, which was shown with direct label-free antibody detection.

890 However, also in works involving metamaterials, the focus is typically pin-pointed on the novelty of the
891 material itself, whereas the presented biosensing evaluation (if presented) is often under-highlighted
892 and relegated to a secondary role. We have no doubt that this situation will change in the next ten to
893 fifteen years, but it will not be until then, that nanoplasmonic sensors will reach a point where their
894 massive use as commercial biosensing platforms becomes attractive. In order to accelerate this
895 technology-transfer process, we argue that more research effort should be focused on one of the most
896 underexposed aspects of nanoplasmonic biosensing*: the surface chemistry*. As discussed in this review,
897 proper biofunctionalization of the surface (with or without complementing microfluidic systems) has led
898 to significant sensitivity enhancements of nanoplasmonic sensing platforms, mainly caused by
899 suppressing non-specific interactions of molecules and forcing biomolecular interactions to take place
900 solely at EM hot-spots of the nanostructures. Examples that point towards this direction are still few in
901 number.

902 Therefore, in order to dethrone conventional SPR sensing (and its well-studied planar surface
903 chemistry), the current knowledge of nanoparticle biofunctionalization should expand drastically. It will
904 not be until then that, when accompanied by low cost and large-scale fabrication techniques,

commercial nanoplasmonic sensing platforms with integrated microfluidics hit the market, and should be considered as viable technological alternatives for conventional SPR sensors.

5. Acknowledgements

We thank the financial support from the national projects MULTIBIOPLAS (TEC2099-08729) and INNBIOD (INNPACTO Subprogram, IPT-2011-1429-010000) from Spanish Ministry of Economy and Competitiveness

6. References

[1] G. Mie, Ann. Phys. , 25 (1908).

[2] H.A. Atwater, A. Polman, Nat Mater, 9 (2010) 205-213.

[3] J.W. Menezes, J. Ferreira, M.J.L. Santos, L. Cescato, A.G. Brolo, Adv Funct Mater, 20 (2010) 3918-3924.

[4] D.K. Gramotnev, S.I. Bozhevolnyi, Nat Photon, 4 (2010) 83-91.

[5] N.G. Khlebtsov, L.A. Dykman, Journal of Quantitative Spectroscopy and Radiative Transfer, 111 (2010) 1-35.

[6] E.Y. Lukianova-Hleb, E.Y. Hanna, J.H. Hafner, D.O. Lapotko, Nanotechnology, 21 (2010) -.

[7] A.G. Brolo, Nat Photon, 6 (2012) 709-713.

[8] K.M. Mayer, J.H. Hafner, Chemical Reviews, 111 (2011) 3828-3857.

[9] B. Sepulveda, P.C. Angelome, L.M. Lechuga, L.M. Liz-Marzan, Nano Today, 4 (2009) 244-251.

[10] E. Petryayeva, U.J. Krull, Anal Chim Acta, 706 (2011) 8-24.

[11] J. Homola, Chemical Reviews, 108 (2008) 462-493.

[12] O.R. Bolduc, L.S. Live, J.-F. Masson, Talanta, 77 (2009) 1680-1687.

[13] M.C. Estevez, M. Alvarez, L.M. Lechuga, Laser & Photonics Reviews, 6 (2012) 463-487.

927 [14] Y. Uludag, I.E. Tothill, Anal Chem (2012).
928 [15] I.E. Sendroiu, L.K. Gifford, A. Luptak, R.M. Corn, J Am Chem Soc, 133 (2011) 4271-4273.
929 [16] W.C. Law, K.T. Yong, A. Baev, P.N. Prasad, ACS Nano, 5 (2011) 4858-4864.
930 [17] W.P. Hall, S.N. Ngatia, R.P. Van Duyne, J Phys Chem C, 115 (2011) 1410-1414.
931 [18] H. Sipova, S.L. Zhang, A.M. Dudley, D. Galas, K. Wang, J. Homola, Anal Chem, 82 (2010) 10110-
932 10115.
933 [19] H. Sipova, T. Springer, J. Homola, Anal Bioanal Chem, 399 (2011) 2343-2350.
934 [20] R. Kashyap, G. Nemova, Journal of Sensors, 2009 (2009).
935 [21] X.D. Hoa, A.G. Kirk, M. Tabrizian, Biosensors and Bioelectronics, 23 (2007) 151-160.
936 [22] M. Piliarik, M. Vala, I. Tichý, J. Homola, Biosensors and Bioelectronics, 24 (2009) 3430-3435.
937 [23] S. Roh, T. Chung, B. Lee, Sensors-Basel, 11 (2011) 1565-1588.
938 [24] M. Piliarik, J.í. Homola, Opt. Express, 17 (2009) 16505-16517.
939 [25] D. Regatos, B. Sepúlveda, D. Fariña, L.G. Carrascosa, L.M. Lechuga, Opt. Express, 19 (2011) 8336-
940 8346.
941 [26] B. Sepulveda, A. Calle, L.M. Lechuga, G. Armelles, Opt Lett, 31 (2006) 1085-1087.
942 [27] R. Slavík, J. Homola, Sensors and Actuators B: Chemical, 123 (2007) 10-12.
943 [28] M. Vala, S. Etheridge, J.A. Roach, J. Homola, Sensors and Actuators B: Chemical, 139 (2009) 59-
944 63.
945 [29] M. Vala, R. Robelek, M. Bocková, J. Wegener, J. Homola, Biosensors and Bioelectronics.
946 [30] T. Springer, M. Piliarik, J. Homola, Sensor Actuat B-Chem, 145 (2010) 588-591.
947 [31] K. Pimkova, M. Bockova, K. Hegnerova, J. Suttnar, J. Cermak, J. Homola, J.E. Dyr, Anal Bioanal
948 Chem, 402 (2012) 381-387.
949 [32] T. Springer, M. Piliarik, J. Homola, Anal Bioanal Chem, 398 (2010) 1955-1961.
950 [33] N.S. Lynn, H. Sipova, P. Adam, J. Homola, Lab on a Chip (2013).

[34] P. Kvasnicka, K. Chadt, M. Vala, M. Bocková, J. Homola, Opt. Lett., 37 (2012) 163-165.

[35] S. Paul, P. Vadgama, A.K. Ray, Nanobiotechnology, IET, 3 (2009) 71-80.

[36] S. Scarano, M. Mascini, A.P.F. Turner, M. Minunni, Biosens Bioelectron, 25 (2010) 957-966.

[37] G. Grasso, R. D'Agata, L. Zanoli, G. Spoto, Microchemical Journal, 93 (2009) 82-86.

[38] M.A. Eddings, J.W. Eckman, C.A. Arana, G.A. Papalia, J.E. Connolly, B.K. Gale, D.G. Myszka, Anal Biochem, 385 (2009) 309-313.

[39] J. Liu, M.A. Eddings, A.R. Miles, R. Bukasov, B.K. Gale, J.S. Shumaker-Parry, Anal Chem, 81 (2009) 4296-4301.

[40] E. Ouellet, C. Lausted, T. Lin, C.W.T. Yang, L. Hood, E.T. Lagally, Lab on a Chip, 10 (2010) 581-588.

[41] L. Malic, B. Cui, T. Veres, M. Tabrizian, Opt Lett, 32 (2007) 3092-3094.

[42] L. Malic, B. Cui, M. Tabrizian, T. Veres, Opt. Express, 17 (2009) 20386-20392.

[43] L. Malic, T. Veres, M. Tabrizian, Biosens Bioelectron, 26 (2011) 2053-2059.

[44] M.R. Jones, K.D. Osberg, R.J. Macfarlane, M.R. Langille, C.A. Mirkin, Chemical Reviews, 111 (2011) 3736-3827.

[45] L.J.E. Anderson, K.M. Mayer, R.D. Fraleigh, Y. Yang, S. Lee, J.H. Hafner, J Phys Chem C, 114 (2010) 11127-11132.

[46] G.W. Lu, L. Hou, T.Y. Zhang, W.Q. Li, J. Liu, P. Perriat, Q.H. Gong, J Phys Chem C, 115 (2011) 22877-22885.

[47] A. Jakab, C. Rosman, Y. Khalavka, J. Becker, A. Trugler, U. Hohenester, C. Sonnichsen, ACS Nano, 5 (2011) 6880-6885.

[48] I. Mannelli, M.P. Marco, Anal Bioanal Chem, 399 (2011) 1923-1923.

[49] X. Le Guevel, F.Y. Wang, O. Stranik, R. Nooney, V. Gubala, C. McDonagh, B.D. MacCraith, J Phys Chem C, 113 (2009) 16380-16386.

[50] D.E. Charles, M. Gara, D. Aherne, D.M. Ledwith, J.M. Kelly, W.J. Blau, M.E. Brennan-Fournet, Plasmonics, 6 (2011) 351-362.

[51] D.E. Charles, D. Aherne, M. Gara, D.M. Ledwith, Y.K. Gun'ko, J.M. Kelly, W.J. Blau, M.E. Brennan-Fournet, ACS Nano, 4 (2010) 55-64.

[52] C.M. Sweeney, C.L. Stender, C.L. Nehl, W. Hasan, K.L. Shuford, T.W. Odom, Small, 7 (2011) 2032-2036.

[53] K.M. Mayer, F. Hao, S. Lee, P. Nordlander, J.H. Hafner, Nanotechnology, 21 (2010).

[54] S. Lee, K.M. Mayer, J.H. Hafner, Anal Chem, 81 (2009) 4450-4455.

[55] X.S. Kou, Z.H. Sun, Z. Yang, H.J. Chen, J.F. Wang, Langmuir, 25 (2009) 1692-1698.

[56] E. Ringe, J.M. McMahon, K. Sohn, C. Cobley, Y.N. Xia, J.X. Huang, G.C. Schatz, L.D. Marks, R.P. Van Duyne, J Phys Chem C, 114 (2010) 12511-12516.

[57] S. Raza, G. Toscano, A.-P. Jauho, N. Mortensen, M. Wubs, Plasmonics 1-7.

[58] S.K. Dondapati, T.K. Sau, C. Hrelescu, T.A. Klar, F.D. Stefani, J. Feldmann, ACS Nano, 4 (2010) 6318-6322.

[59] G.K. Joshi, P.J. McClory, S. Dolai, R. Sardar, J Mater Chem, 22 (2012) 923-931.

[60] M.B. Cortie, A.M. McDonagh, Chemical Reviews, 111 (2011) 3713-3735.

[61] T.Y. Olson, A.M. Schwartzberg, C.A. Orme, C.E. Talley, B. O'Connell, J.Z. Zhang, J Phys Chem C, 112 (2008) 6319-6329.

[62] I.E. Sendroiu, M.E. Warner, R.M. Corn, Langmuir, 25 (2009) 11282-11284.

[63] J.R. Cole, N.A. Mirin, M.W. Knight, G.P. Goodrich, N.J. Halas, J Phys Chem C, 113 (2009) 12090-12094.

[64] R. Bardhan, S. Mukherjee, N.A. Mirin, S.D. Levit, P. Nordlander, N.J. Halas, J Phys Chem C, 114 (2010) 7378-7383.

997 [65] T.D. Schladt, M.I. Shukoor, K. Schneider, M.N. Tahir, F. Natalio, I. Ament, J. Becker, F.D. Jochum,
998 S. Weber, O. Kohler, P. Theato, L.M. Schreiber, C. Sonnichsen, H.C. Schroder, W.E.G. Muller, W. Tremel,
999 Angew Chem Int Edit, 49 (2010) 3976-3980.
1000 [66] F. López-Tejeira, R. Paniagua-Domínguez, J.A. Sánchez-Gil, ACS Nano, 6 (2012) 8989-8996.
1001 [67] L. Guo, Y. Yin, R. Huang, B. Qiu, Z. Lin, H.-H. Yang, J. Li, G. Chen, Lab on a Chip, 12 (2012) 3901-
1002 3906.
1003 [68] S.M. Marinakos, S.H. Chen, A. Chilkoti, Anal Chem, 79 (2007) 5278-5283.
1004 [69] S.R. Beeram, F.P. Zamborini, ACS Nano, 4 (2010) 3633-3646.
1005 [70] J.P. Camden, J.A. Dieringer, J. Zhao, R.P. Van Duyne, Accounts Chem Res, 41 (2008) 1653-1661.
1006 [71] C.L. Haynes, R.P. Van Duyne, J Phys Chem B, 105 (2001) 5599-5611.
1007 [72] S.L. Zhu, C.L. Du, Y.Q. Fu, Opt Mater, 31 (2009) 769-774.
1008 [73] H. Fredriksson, Y. Alaverdyan, A. Dmitriev, C. Langhammer, D.S. Sutherland, M. Zaech, B.
1009 Kasemo, Adv Mater, 19 (2007) 4297-+.
1010 [74] B.D. Lucas, J.S. Kim, C. Chin, L.J. Guo, Adv Mater, 20 (2008) 1129-+.
1011 [75] J. Henzie, J. Lee, M.H. Lee, W. Hasan, T.W. Odom, Annu Rev Phys Chem, 60 (2009) 147-165.
1012 [76] M.H. Lee, M.D. Huntington, W. Zhou, J.C. Yang, T.W. Odom, Nano Lett, 11 (2011) 311-315.
1013 [77] J. McPhillips, C. McClatchey, T. Kelly, A. Murphy, M.P. Jonsson, G.A. Wurtz, R.J. Winfield, R.J.
1014 Pollard, J Phys Chem C, 115 (2011) 15234-15239.
1015 [78] A. Cattoni, P. Ghenuche, A.M. Haghiri-Gosnet, D. Decanini, J. Chen, J.L. Pelouard, S. Collin, Nano
1016 Letters, 11 (2011) 3557-3563.
1017 [79] H. Im, S.H. Lee, N.J. Wittenberg, T.W. Johnson, N.C. Lindquist, P. Nagpal, D.J. Norris, S.H. Oh, ACS
1018 Nano, 5 (2011) 6244-6253.
1019 [80] C.C. Liang, M.Y. Liao, W.Y. Chen, T.C. Cheng, W.H. Chang, C.H. Lin, Opt Express, 19 (2011) 4768-
1020 4776.

[81] S.W. Lee, K.S. Lee, J. Ahn, J.J. Lee, M.G. Kim, Y.B. Shin, ACS Nano, 5 (2011) 897-904.

[82] S.H. Lee, B. Cho, S. Yoon, H. Jeong, S. Jon, G.Y. Jung, B.K. Cho, T. Lee, W.B. Kim, ACS Nano, 5 (2011) 5543-5551.

[83] M.H. Lee, J.Y. Lin, T.W. Odom, Angew Chem Int Ed Engl, 49 (2010) 3057-3060.

[84] O. Vazquez-Mena, T. Sannomiya, L.G. Villanueva, J. Voros, J. Brugger, ACS Nano, 5 (2011) 844-853.

[85] S. Aksu, A.A. Yanik, R. Adato, A. Artar, M. Huang, H. Altug, Nano Letters, 10 (2010) 2511-2518.

[86] O. Vazquez-Mena, T. Sannomiya, M. Tosun, L.G. Villanueva, V. Savu, J. Voros, J. Brugger, ACS Nano (2012).

[87] S. Aksu, M. Huang, A. Artar, A.A. Yanik, S. Selvarasah, M.R. Dokmeci, H. Altug, Adv Mater, 23 (2011) 4422-+.

[88] A.V. Kabashin, P. Evans, S. Pastkovsky, W. Hendren, G.A. Wurtz, R. Atkinson, R. Pollard, V.A. Podolskiy, A.V. Zayats, Nat Mater, 8 (2009) 867-871.

[89] J. McPhillips, A. Murphy, M.P. Jonsson, W.R. Hendren, R. Atkinson, F. Hook, A.V. Zayats, R.J. Pollard, ACS Nano, 4 (2010) 2210-2216.

[90] T.-Y. Chang, M. Huang, A.A. Yanik, H.-Y. Tsai, P. Shi, S. Aksu, M.F. Yanik, H. Altug, Lab on a Chip (2011).

[91] B. Yan, S.V. Boriskina, B.M. Reinhard, J Phys Chem C, 115 (2011) 24437-24453.

[92] M.A. Otte, B. Sepulveda, W.H. Ni, J.P. Juste, L.M. Liz-Marzan, L.M. Lechuga, ACS Nano, 4 (2010) 349-357.

[93] J. Becker, A. Trugler, A. Jakab, U. Hohenester, C. Sonnichsen, Plasmonics, 5 (2010) 161-167.

[94] S.D. Liu, Z. Yang, R.P. Liu, X.Y. Li, J Phys Chem C, 115 (2011) 24469-24477.

[95] K. Lodewijks, W. Van Roy, G. Borghs, L. Lagae, P. Van Dorpe, Nano Letters, 12 (2012) 1655-1659.

1044 [96] B. Paivanranta, H. Merbold, R. Giannini, L. Buchi, S. Gorelick, C. David, J.F. Loffler, T. Feurer, Y.
1045 Ekinci, ACS Nano, 5 (2011) 6374-6382.
1046 [97] M. Svedendahl, S. Chen, A. Dmitriev, M. Kall, Nano Letters, 9 (2009) 4428-4433.
1047 [98] J. Ye, P. Van Dorpe, Plasmonics, 6 (2011) 665-671.
1048 [99] Y.K. Gao, Q.Q. Gan, Z.M. Xin, X.H. Cheng, F.J. Bartoli, ACS Nano, 5 (2011) 9836-9844.
1049 [100] P. Offermans, M.C. Schaafsma, S.R.K. Rodriguez, Y.C. Zhang, M. Crego-Calama, S.H. Brongersma,
1050 J.G. Rivas, ACS Nano, 5 (2011) 5151-5157.
1051 [101] P. Kvasnicka, J. Homola, Biointerphases, 3 (2008) Fd4-Fd11.
1052 [102] L. Tian, E. Chen, N. Gandra, A. Abbas, S. Singamaneni, Langmuir (2012).
1053 [103] J.S. Sekhon, S.S. Verma, Plasmonics, 6 (2011) 163-169.
1054 [104] H.J. Chen, X.S. Kou, Z. Yang, W.H. Ni, J.F. Wang, Langmuir, 24 (2008) 5233-5237.
1055 [105] A.E. Cetin, H. Altug, ACS Nano (2012).
1056 [106] N. Verellen, P. Van Dorpe, C.J. Huang, K. Lodewijks, G.A.E. Vandenbosch, L. Lagae, V.V.
1057 Moshchalkov, Nano Letters, 11 (2011) 391-397.
1058 [107] M. Piliarik, P. Kvasnicka, N. Galler, J.R. Krenn, J. Homola, Opt Express, 19 (2011) 9213-9220.
1059 [108] L. Feuz, P. Jonsson, M.P. Jonsson, F. Hook, ACS Nano, 4 (2010) 2167-2177.
1060 [109] L. Feuz, M.P. Jonsson, F. Hook, Nano Letters, 12 (2012) 873-879.
1061 [110] S.R. Beeram, F.P. Zamborini, J Am Chem Soc, 131 (2009) 11689-+.
1062 [111] S.R. Beeram, F.P. Zamborini, J Phys Chem C, 115 (2011) 7364-7371.
1063 [112] M.A. Otte, M.C. Estevez, L.G. Carrascosa, A.B. Gonzalez-Guerrero, L.M. Lechuga, B. Sepulveda, J
1064 Phys Chem C, 115 (2011) 5344-5351.
1065 [113] T. Siegfried, Y. Ekinci, O.J.F. Martin, H. Sigg, ACS Nano, 7 (2013) 2751-2757.
1066 [114] T.G. Habteyes, S. Dhuey, E. Wood, D. Gargas, S. Cabrini, P.J. Schuck, A.P. Alivisatos, S.R. Leone,
1067 ACS Nano (2012).

[115] M.M. Miller, A.A. Lazarides, J Phys Chem B, 109 (2005) 21556-21565.

[116] B. Brian, B. Sepulveda, Y. Alaverdyan, L.M. Lechuga, M. Kall, Opt Express, 17 (2009) 2015-2023.

[117] A. Dmitriev, C. Hagglund, S. Chen, H. Fredriksson, T. Pakizeh, M. Kall, D.S. Sutherland, Nano Letters, 8 (2008) 3893-3898.

[118] W. Knoben, S.H. Brongersma, M. Crego-Calama, Nanotechnology, 22 (2011).

[119] M. Piliarik, H. Sipova, P. Kvasnicka, N. Galler, J.R. Krenn, J. Homola, Opt Express, 20 (2012) 672-680.

[120] H. Sipova, D. Vrba, J. Homola, Anal Chem, 84 (2012) 30-33.

[121] J.A. Fan, K. Bao, J.B. Lassiter, J. Bao, N.J. Halas, P. Nordlander, F. Capasso, Nano Letters, 12 (2012) 2817-2821.

[122] P.E. Sheehan, L.J. Whitman, Nano Letters, 5 (2005) 803-807.

[123] P.R. Nair, M.A. Alam, Appl Phys Lett, 88 (2006) 233120-233123.

[124] T.M. Squires, R.J. Messinger, S.R. Manalis, Nat Biotech, 26 (2008) 417-426.

[125] I. Ament, J. Prasad, A. Henkel, S. Schmachtel, C. Sonnichsen, Nano Letters, 12 (2012) 1092-1095.

[126] P. Zijlstra, P.M.R. Paulo, M. Orrit, Nat Nano, 7 (2012) 379-382.

[127] P. Zijlstra, P.M.R. Paulo, K. Yu, Q.-H. Xu, M. Orrit, Angewandte Chemie International Edition (2012) n/a-n/a.

[128] J.M. Bingham, K.A. Willets, N.C. Shah, D.Q. Andrews, R.P. Van Duyne, The Journal of Physical Chemistry C, 113 (2009) 16839-16842.

[129] K.H. Chen, J. Hobley, Y.L. Foo, X.D. Su, Lab on a Chip, 11 (2011) 1895-1901.

[130] L.H. Guo, A.R. Ferhan, K. Lee, D.H. Kim, Anal Chem, 83 (2011) 2605-2612.

[131] T. Sannomiya, C. Hafner, J. Voros, Nano Letters, 8 (2008) 3450-3455.

[132] S. Chen, M. Svedendahl, R.P. Van Duyne, M. Kall, Nano Letters, 11 (2011) 1826-1830.

[133] A.D. McFarland, R.P. Van Duyne, Nano Letters, 3 (2003) 1057-1062.

[134] G. Raschke, S. Kowarik, T. Franzl, C. Sönnichsen, T.A. Klar, J. Feldmann, A. Nichtl, K. Kürzinger, Nano Letters, 3 (2003) 935-938.

[135] G.J. Nusz, S.M. Marinakos, A.C. Curry, A. Dahlin, F. Hook, A. Wax, A. Chilkoti, Anal Chem, 80 (2008) 984-989.

[136] T. Rindzevicius, Y. Alaverdyan, A. Dahlin, F. Höök, D.S. Sutherland, M. Käll, Nano Letters, 5 (2005) 2335-2339.

[137] W.S. Hwang, P.L. Truong, S.J. Sim, Anal Biochem, 421 (2012) 213-218.

[138] P.L. Truong, C. Cao, S. Park, M. Kim, S.J. Sim, Lab on a Chip, 11 (2011) 2591-2597.

[139] L.H. Guo, X.D. Zhou, D.H. Kim, Biosens Bioelectron, 26 (2011) 2246-2251.

[140] T. Huang, P.D. Nallathamby, X.H.N. Xu, J Am Chem Soc, 130 (2008) 17095-17105.

[141] M.S. Song, S.P. Choi, J. Lee, Y.J. Kwon, S.J. Sim, Adv Mater, 25 (2013) 1265-1269.

[142] R. Roy, S. Hohng, T. Ha, Nat Meth, 5 (2008) 507-516.

[143] A.J. Haes, L. Chang, W.L. Klein, R.P. Van Duyne, J Am Chem Soc, 127 (2005) 2264-2271.

[144] A.J. Haes, W.P. Hall, L. Chang, W.L. Klein, R.P. Van Duyne, Nano Letters, 4 (2004) 1029-1034.

[145] K.M. Mayer, S. Lee, H. Liao, B.C. Rostro, A. Fuentes, P.T. Scully, C.L. Nehl, J.H. Hafner, ACS Nano, 2 (2008) 687-692.

[146] S. Chen, M. Svedendahl, M. Kall, L. Gunnarsson, A. Dmitriev, Nanotechnology, 20 (2009).

[147] H.M. Hiep, T. Endo, K. Kerman, M. Chikae, D.K. Kim, S. Yamamura, Y. Takamura, E. Tamiya, Science and Technology of Advanced Materials, 8 (2007) 331-338.

[148] T. Endo, S. Yamamura, K. Kerman, E. Tamiya, Anal Chim Acta, 614 (2008) 182-189.

[149] M. Vestergaard, K. Kerman, D.K. Kim, H.M. Hiep, E. Tamiya, Talanta, 74 (2008) 1038-1042.

[150] H.M. Hiep, T. Endo, M. Saito, M. Chikae, D.K. Kim, S. Yamamura, Y. Takamura, E. Tamiya, Anal Chem, 80 (2008) 1859-1864.

[151] H.M. Hiep, M. Saito, Y. Nakamura, E. Tamiya, Anal Bioanal Chem, 396 (2010) 2575-2581.

[152] T. Endo, K. Kerman, N. Nagatani, H.M. Hiepa, D.-K. Kim, Y. Yonezawa, K. Nakano, E. Tamiya, Anal Chem, 78 (2006) 6465-6475.

[153] S. Zheng, D.K. Kim, T.J. Park, S.J. Lee, S.Y. Lee, Talanta, 82 (2010) 803-809.

[154] T.J. Park, S.J. Lee, D.-K. Kim, N.S. Heo, J.Y. Park, S.Y. Lee, Talanta, 89 (2012) 246-252.

[155] S.Y. Yoo, D.K. Kim, T.J. Park, E.K. Kim, E. Tamiya, S.Y. Lee, Anal Chem, 82 (2010) 1349-1357.

[156] D.-K. Kim, S.M. Yoo, T.J. Park, H. Yoshikawa, E. Tamiya, J.Y. Park, S.Y. Lee, Anal Chem, 83 (2011) 6215-6222.

[157] L. Guo, D. Wang, Y. Xu, B. Qiu, Z. Lin, H. Dai, H.-H. Yang, G. Chen, Biosensors and Bioelectronics, 47 (2013) 199-205.

[158] W.P. Hall, J. Modica, J. Anker, Y. Lin, M. Mrksich, R.P. Van Duynet, Nano Letters, 11 (2011) 1098-1105.

[159] J. Zhao, A. Das, G.C. Schatz, S.G. Sligar, R.P. Van Duyne, J Phys Chem C, 112 (2008) 13084-13088.

[160] A. Das, J. Zhao, G.C. Schatz, S.G. Sligar, R.P. Van Duyne, Anal Chem, 81 (2009) 3754-3759.

[161] T.W. Ebbesen, H.J. Lezec, H.F. Ghaemi, T. Thio, P.A. Wolff, Nature, 391 (1998) 667-669.

[162] Y. Alaverdyan, B. Sepulveda, L. Eurenius, E. Olsson, M. Kall, Nat Phys, 3 (2007) 884-889.

[163] J. Ferreira, M.J.L. Santos, M.M. Rahman, A.G. Brolo, R. Gordon, D. Sinton, E.M. Girotto, J Am Chem Soc, 131 (2009) 436-+.

[164] J.C. Sharpe, J.S. Mitchell, L. Lin, H. Sedoglavich, R.J. Blaikie, Anal Chem, 80 (2008) 2244-2249.

[165] R. Gordon, D. Sinton, K.L. Kavanagh, A.G. Brolo, Accounts Chem Res, 41 (2008) 1049-1057.

[166] H. Im, J.N. Sutherland, J.A. Maynard, S.H. Oh, Anal Chem, 84 (2012) 1941-1947.

[167] T. Sannomiya, O. Scholder, K. Jefimovs, C. Hafner, A.B. Dahlin, Small, 7 (2011) 1653-1663.

[168] M.P. Murray-Methot, M. Ratel, J.F. Masson, J Phys Chem C, 114 (2010) 8268-8275.

[169] C. Escobedo, Lab on a Chip (2013).

[170] C. Escobedo, Y.-W. Chou, M. Rahman, X. Duan, R. Gordon, D. Sinton, A. Brolo, J. Ferreira, Analyst (2013).

[171] J. Ji, J.G. O'Connell, D.J.D. Carter, D.N. Larson, Anal Chem, 80 (2008) 2491-2498.

[172] L.S. Live, O.R. Bolduc, J.F. Masson, Anal Chem, 82 (2010) 3780-3787.

[173] M. Couture, L.S. Live, A. Dhawan, J.-F. Masson, Analyst (2012).

[174] - - , J.-F. Masson, The Journal of Physical Chemistry C, 113 (2008) 40-44.

[175] R. Gordon, A.G. Brolo, D. Sinton, K.L. Kavanagh, Laser & Photonics Reviews, 4 (2010) 311-335.

[176] J.C. Yang, H.W. Gao, J.Y. Suh, W. Zhou, M.H. Lee, T.W. Odom, Nano Letters, 10 (2010) 3173-3178.

[177] B. Sepulveda, Y. Alaverdyan, J. Alegret, M. Kall, P. Johansson, Opt Express, 16 (2008) 5609-5616.

[178] A.B. Dahlin, M.P. Jonsson, F. Hook, Adv Mater, 20 (2008) 1436-+.

[179] M.P. Jonsson, P. Jönsson, A.B. Dahlin, F. Höök, Nano Letters, 7 (2007) 3462-3468.

[180] N.J. Wittenberg, H. Im, X. Xu, B. Wootla, J. Watzlawik, A.E. Warrington, M. Rodriguez, S.-H. Oh, Anal Chem, 84 (2012) 6031-6039.

[181] D. Sinton, R. Gordon, A.G. Brolo, Microfluidics and Nanofluidics, 4 (2008) 107-116.

[182] F. Eftekhari, C. Escobedo, J. Ferreira, X.B. Duan, E.M. Girotto, A.G. Brolo, R. Gordon, D. Sinton, Anal Chem, 81 (2009) 4308-4311.

[183] C. Escobedo, A.G. Brolo, R. Gordon, D. Sinton, Anal Chem, 82 (2010) 10015-10020.

[184] C. Escobedo, A.G. Brolo, R. Gordon, D. Sinton, Nano Letters, 12 (2012) 1592-1596.

[185] M. Huang, A.A. Yanik, T.Y. Chang, H. Altug, Opt Express, 17 (2009) 24224-24233.

[186] A.A. Yanik, M. Huang, A. Artar, T.Y. Chang, H. Altug, Appl Phys Lett, 96 (2010).

[187] A.A. Yanik, M. Huang, O. Kamohara, A. Artar, T.W. Geisbert, J.H. Connor, H. Altug, Nano Letters, 10 (2010) 4962-4969.

[188] M.P. Jonsson, A.B. Dahlin, L. Feuz, S. Petronis, F. Hook, Anal Chem, 82 (2010) 2087-2094.

[189] http://www.lamdagen.com

[190] C.J. Huang, K. Bonroy, G. Reekmans, W. Laureyn, K. Verhaegen, I. De Vlaminck, L. Lagae, G. Borghs, Biomedical Microdevices, 11 (2009) 893-901.

[191] C.J. Huang, K. Bonroy, G. Reekman, K. Verstreken, L. Lagae, G. Borghs, Microelectron Eng, 86 (2009) 2437-2441.

[192] P. Neuzil, J. Reboud, Anal Chem, 80 (2008) 6100-6103.

[193] G. Cappi, E. Accastelli, V. Cantale, M.A. Rampi, L. Benini, C. Guiducci, Sensors and Actuators B: Chemical, 176 (2013) 225-231.

[194] F. Mazzotta, G.L. Wang, C. Hagglund, F. Hook, M.P. Jonsson, Biosens Bioelectron, 26 (2010) 1131-1136.

[195] K. Hedsten, J. Fonollosa, P. Enoksson, P. Modh, J. Bengtsson, D.S. Sutherland, A. Dmitriev, Anal Chem, 82 (2010) 1535-1539.

[196] J.A. Ruemmele, W.P. Hall, L.K. Ruvuna, R.P. Van Duyne, Anal Chem (2013).

[197] A. De Leebeeck, L.K.S. Kumar, V. de Lange, D. Sinton, R. Gordon, A.G. Brolo, Anal Chem, 79 (2007) 4094-4100.

[198] N.C. Lindquist, A. Lesuffleur, H. Im, S.-H. Oh, Lab on a Chip, 9 (2009) 382-387.

[199] S.H. Lee, N. Lindquist, N.J. Wittenberg, L.R. Jordan, S.-H. Oh, Lab on a Chip (2012).

[200] L. Malic, K. Morton, L. Clime, T. Veres, Lab on a Chip, 13 (2013) 798-810.

[201] J.A. Fan, C.H. Wu, K. Bao, J.M. Bao, R. Bardhan, N.J. Halas, V.N. Manoharan, P. Nordlander, G. Shvets, F. Capasso, Science, 328 (2010) 1135-1138.

[202] N.J. Halas, S. Lal, W.-S. Chang, S. Link, P. Nordlander, Chemical Reviews, 111 (2011) 3913-3961.

[203] W. Zhou, T.W. Odom, Nat Nanotechnol, 6 (2011) 423-427.

[204] C.H. Wu, A.B. Khanikaev, R. Adato, N. Arju, A.A. Yanik, H. Altug, G. Shvets, Nat Mater, 11 (2012) 69-75.

[205] A.A. Yanik, A.E. Cetin, M. Huang, A. Artar, S.H. Mousavi, A. Khanikaev, J.H. Connor, G. Shvets, H. Altug, P Natl Acad Sci USA, 108 (2011) 11784-11789.

[206] S.P. Zhang, K. Bao, N.J. Halas, H.X. Xu, P. Nordlander, Nano Letters, 11 (2011) 1657-1663.

[207] S.-H. Wu, K.-L. Lee, A. Chiou, X. Cheng, P.-K. Wei, Small (2013) n/a-n/a.

[208] F. Hao, P. Nordlander, Y. Sonnefraud, P. Van Dorpe, S.A. Maier, ACS Nano, 3 (2009) 643-652.

[209] F. Hao, Y. Sonnefraud, P. Van Dorpe, S.A. Maier, N.J. Halas, P. Nordlander, Nano Letters, 8 (2008) 3983-3988.

[210] X.M. Bendana, G. Lozano, G. Pirruccio, J.G. Rivas, F.J.G. de Abajo, Opt Express, 21 (2013) 5636-5642.

[211] Y.Z. Chu, E. Schonbrun, T. Yang, K.B. Crozier, Appl Phys Lett, 93 (2008).

[212] E.M. Hicks, S.L. Zou, G.C. Schatz, K.G. Spears, R.P. Van Duyne, L. Gunnarsson, T. Rindzevicius, B. Kasemo, M. Kall, Nano Letters, 5 (2005) 1065-1070.

[213] V.G. Kravets, F. Schedin, A.N. Grigorenko, Phys Rev Lett, 101 (2008).

[214] M.A. Otte, M.C. Estevez, D. Regatos, L.M. Lechuga, B. Sepulveda, ACS Nano, 5 (2011) 9179-9186.

[215] M.P. Kreuzer, R. Quidant, J.P. Salvador, M.P. Marco, G. Badenes, Anal Bioanal Chem, 391 (2008) 1813-1820.

[216] S.-H. Yeom, M.-E. Han, B.-H. Kang, K.-J. Kim, H. Yuan, N.-S. Eum, S.-W. Kang, Sensors and Actuators B: Chemical, 177 (2013) 376-383.

[217] W. Zhou, Y.Y. Ma, H.A. Yang, Y. Ding, X.G. Luo, Int J Nanomed, 6 (2011) 381-386.

Tables

Table 1. Examples of LSPR biosensing assays

Substrate	Features	Bioassay	Sensitivity/LOD	Ref.
Au Nanoholes	• Flow-through nanoholes; static measurements in air	• Viruses (VSV, Ebola and Vaccinia) • Direct detection with Ab oriented via Protein G • Cell-growth media measurements	10^6 -10^9 pfu/mL-	[187]
Au Nanoholes	• Flow-through nanoholes ; real-time measurements • Controlled gold surface modification preserving SiN from nospecific adsorption	• Neutravidin binding • Biotin-PEG immobilized on gold	n.r.	[188]
Au Nanoholes	• Non-suspended nanoholes. • Flow real-time measurements • SiO_x layer on top of gold	• Study of supported lipid bilayer (SLB) formation • Protein binding • Conformational changes	n.r.	[179]
Au Nanoholes	• Non-suspended nanoholes.	• Autoantibodies detection on SLB	n.r.	[180]

	• Flow real-time measurements • SiO_2 layer on top of gold	• Complete kinetics characterization		
Au nanodisks	• Flow real-time measurements • No specificity studies • Not detailed assay optimization	• Extracellular adherence protein (EAP) • Direct detection with Ab	8pM (estimated)	[146]
		• Prostate specific antigen (PSA) • Direct detection with Ab	1pM (estimated)	
Au nanodisks	• Flow cell to deliver samples • Static measurements after incubation • No specificity studies • Not detailed assay optimization	• Prostate specific antigen (PSA) • Direct detection with Ab	>280 pM	[81]
		• Sandwich assay + substrate precipitation	83 fM (3pg/mL)	
Au capped NPs	• Static measurements after incubation	• Casein detection in milk • Direct detection with Ab oriented via Protein G	10 ng/mL	[147]
Au capped NPs	• Static measurements after incubation	• IL-2 secreted from cells after stimulation • Direct detection with Ab Oriented via Protein A	10 pg/mL	[148]
Au capped NPs	• Static measurements after incubation	• Tau protein detection in • Direct detection with Ab oriented via Protein G	10 pg/mL	[149]
Au capped NPs	• Static measurements after incubation	• Melittin (peptide toxin)	10 ng/mL	[150]

		• Interaction study with Hybrid bilayer membrane (HBM)		
Au-capped NPs	• Static measurements after incubation	• Fibrinogen • Direct detection with Ab oriented via RNA aptamer which recognizes Fc fraction	0.1 ng/mL	[151]
Au-capped NPs (Multispot)	• Static measurements after incubation • Sequential spot measurement	• Antibody against Avian influenza antigen (AIa) • Gold binding preptide-AIa fusion protein (GBP-AIa) immobilized on the surface	1 pg/mL	[154]
Au-capped NPs (Multispot)	• Static measurements after incubation • Sequential spot measurement	• Hepatitis B (HB) antigen (HBsAg) detection • GBP-scFv fusion protein immobilized on the surface	100 pg/mL	[153]
		• Anti-HBsAg deetection • GBP-HBS-Ag fusion protein immobilized on the surface	1 pg/mL	
Au-capped NPs (Multispot)	• Static measurements after incubation • Sequential spot measurement • Real samples analysis	• Single point mutation detection of BIGH3 gene (related to Corneal Dystrophy) • Complementary sequence immobilized	1pM target DNA	[155]

Cu-capped NPs (Multispot)	• Static measurements after incubation • Sequential spot measurement • Real samples (Clinical Isolates)	• Bacterial DNA detection • Complementary sequence immobilized	10 fM target DNA	[156]
Au NPs	• Static measurements after incubation	• Stazonolol (steroidal hormone) detection • Indirect competitive immunoassay with specific Ab	2.4 nM	[215]
Au deposited on nanoporous structure (Anodicaluminum oxide substrates AAO)	• Static measurements after incubation	• CRP detection • Direct detection with Antibody immobilized	1 fg/mL	[216]
Ag NPs	• Static measurements	• P450 Cytochrome (CYP3A4) interaction with drugs CYP3A4 stablized and immobilized on NP	Qualitative	[160]
Ag nanotriangles	• Static measurements after incubation • Serum samples • No optimization	• Detection of p53 • Direct detection with Antibody immobilized	n.r	[217]
Au nanorods	• Flow cell to deliver samples	• Enantioselective detection of RS-melagatran	0.9 nM of RS-	[67]

	• Static measurements after incubation • Reproducibility studies	• Chiral recognition using human α.thrombin • Serum matrix studies	melagatran	
Au nanorods	• Flow cell to deliver samples • Static measurements after incubation • Reproducibility and accuracy studies	• Chiral discrimination of racemic mixture of TNA • Protein immobilized on the surface or • Specific antibody immobilized on the surface	20-100 nM of chiral TNA(depending on the receptor)	[157]
Ag nanoprisms	• Flow real time measurements • Accurate surface immobilization for correct orientation	• Conformational changes of calmodulin upon ion interaction • Cqalmodulin-ligand interaction study • Kinetics studies of the conformational change	600 fmol Ca^{2+}/cm^2 23 μM of Ca^2	[158]

Figure Legends

Figure 1. Schematics showing the detection principle of plasmonic biosensors based on (A) Surface Plasmon Polaritons (SPPs or SPRs) propagating along the interface of a metal and a dielectric. (B) Localized Surface Plasmon Resonances (LSPRs) strongly confined to the surface of sub-wavelength metal nanostructures.

Figure 2. Scientific publications centered on the topic of nanoplasmonics (1990-2012). Source: Web of Knowledge.

Figure 3. Diagrams illustrating nanostructure-based biosensing setups: (A) Extinction measurements, (B) Dark-field microscopy and (C) Total Internal Reflection (TIR) microscopy.

Figure 4. Examples of controlled directed functionalization of metal nanostructures (A) Gold nanoholes of TiO_2 functionalized with different surface-selective compounds. The control on the modification of the most sensitive material (gold) leads to signal enhancement [108]. (B) Controlled binding on the hotspots (between two gold nanodisks) and comparison with whole gold nanodisk surface. A 4x signal per molecule enhancement is achieved [109]. (C) Wavelength shift achieved on gold nanoplates after IgG binding on the terrace or in the edges (more sensitive areas) [111]. Reproduced from [108, 109, 111]. Copyright (2010, 2012 and 2011) American Chemical Society.

Figure 5. Schematic representation of short-range ordered arrays of gold nanodisks located on isotropic dielectric pillars, providing a strategy that can be used to increase the refractometric sensing performance of these nanostructures [112]. Single stranded DNA molecules attached to the nanodisks are used as receptor probes for the specific detection of complementary DNA strands.

Figure 6. Examples of integrated LSPR systems. (A) Microfluidics with two cells, the setup scheme and the automated sample delivery system [191]. (B) Compact small size transmission based LSPR using three LEDs as light source. The system incorporates the sample and photo detector [193]. (C) Palm-size reflectance-based LSPR with four LEDs as light source and a photodiode as detector. It incorporates a LCD touch screen display [192]. Reproduced from [191-193],

Figures

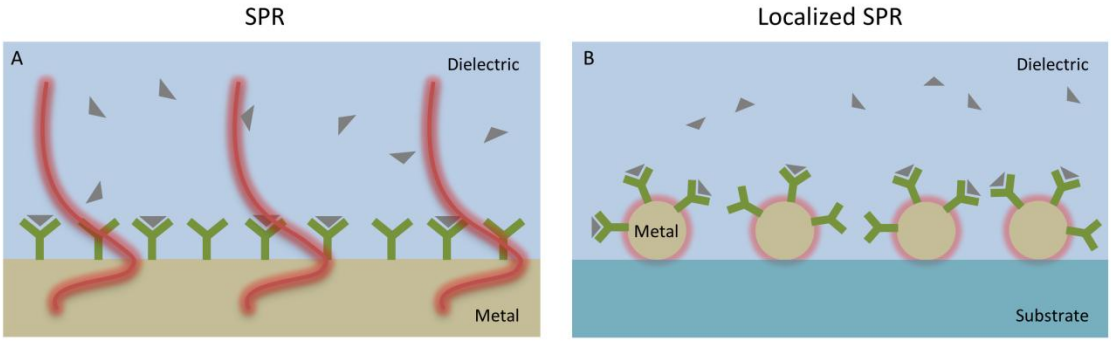

Figure 1

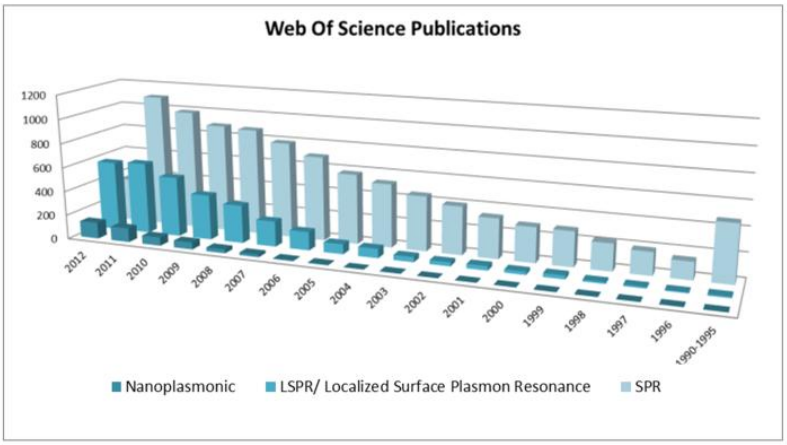
Web Of Science Publications
1200
1000
800
600
400
200
0
2012
2011
2010
2009
2008
2007
2006
2005
2004
2003
2002
2001
2000
1999
1998
1997
1996
1990-1995
Nanoplasmonic
LSPR/ Localized Surface Plasmon Resonance
SPR

Figure 2

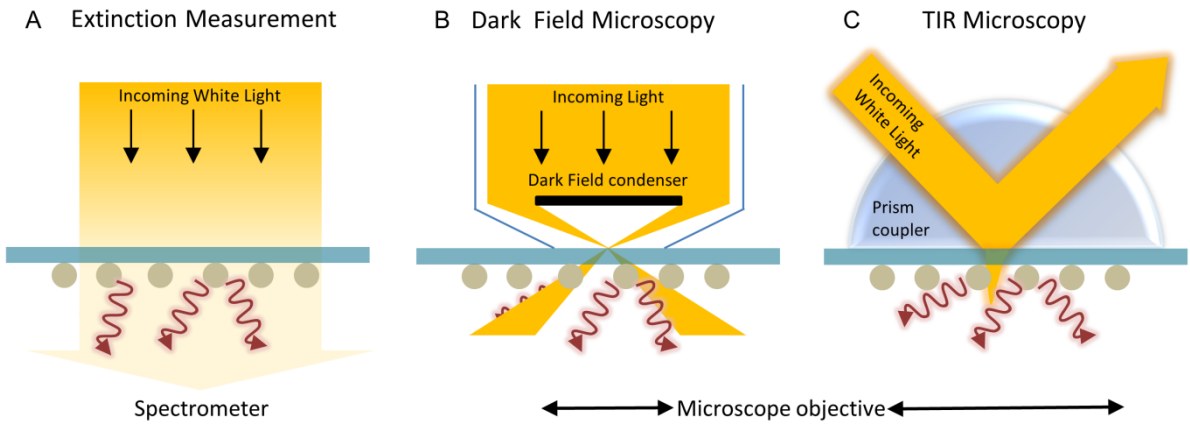
A Extinction Measurement
Incoming White Light
Spectrometer
B Dark Field Microscopy
Incoming Light
Dark Field condenser
Microscope objective
C TIR Microscopy
Incoming White Light
Prism coupler

Figure 3

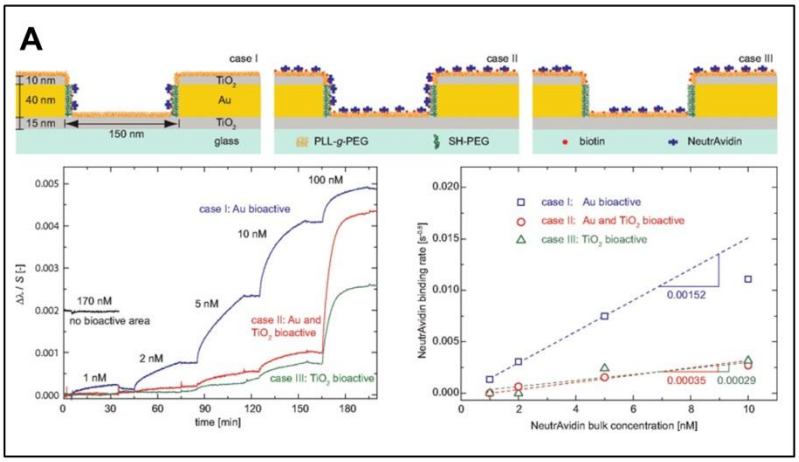
A
case I
case II
case III
10 nm
40 nm
15 nm
150 nm
TiO2
Au
TiO2
glass
PLL-g-PEG
SH-PEG
biotin
NeutrAvidin
100 nM
10 nM
5 nM
2 nM
1 nM
170 nM
no bioactive area
case I: Au bioactive
case II: Au and TiO2 bioactive
case III: TiO2 bioactive
Δλ / S [-]
time [min]
NeutrAvidin binding rate [s-1M-1]
0.00152
0.00035
0.00029
NeutrAvidin bulk concentration [nM]

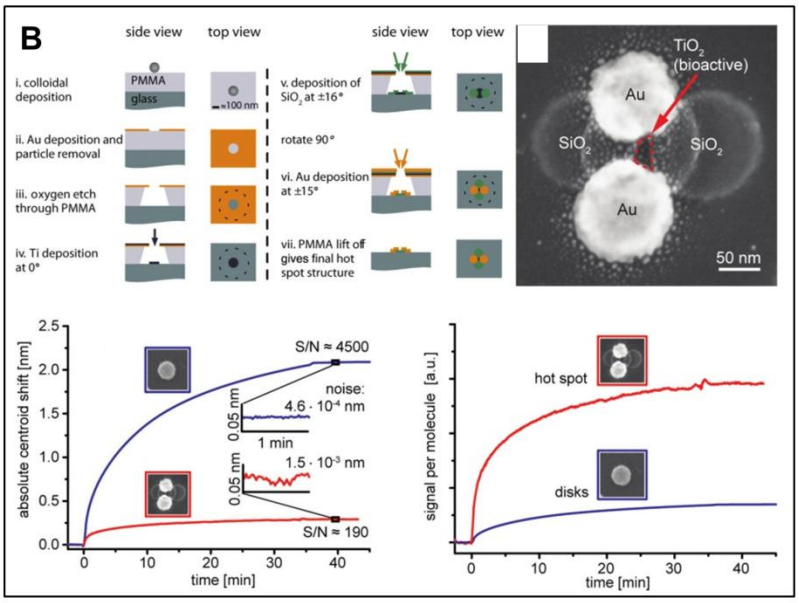
B
side view
top view
i. colloidal deposition
PMMA
glass
≈100 nm
ii. Au deposition and particle removal
iii. oxygen etch through PMMA
iv. Ti deposition at 0°
v. deposition of SiO2 at ±16°
rotate 90°
vi. Au deposition at ±15°
vii. PMMA lift off gives final hot spot structure
TiO2 (bioactive)
Au
SiO2
SiO2
Au
50 nm
absolute centroid shift [nm]
S/N ≈ 4500
noise:
4.6 · 10-4 nm
0.05 nm
1 min
1.5 · 10-3 nm
S/N ≈ 190
time [min]
signal per molecule [a.u.]
hot spot
disks
time [min]

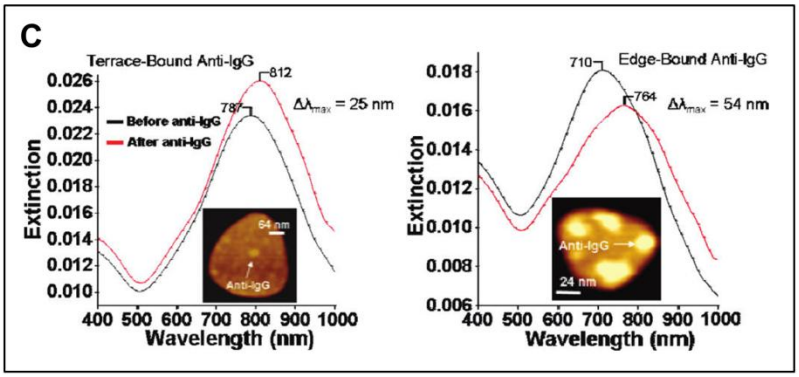
C
Terrace-Bound Anti-IgG
812
787
Δλmax = 25 nm
Before anti-IgG
After anti-IgG
64 nm
Anti-IgG
Extinction
Wavelength (nm)
Edge-Bound Anti-IgG
710
764
Δλmax = 54 nm
Anti-IgG
24 nm
Extinction
Wavelength (nm)

Figure 4

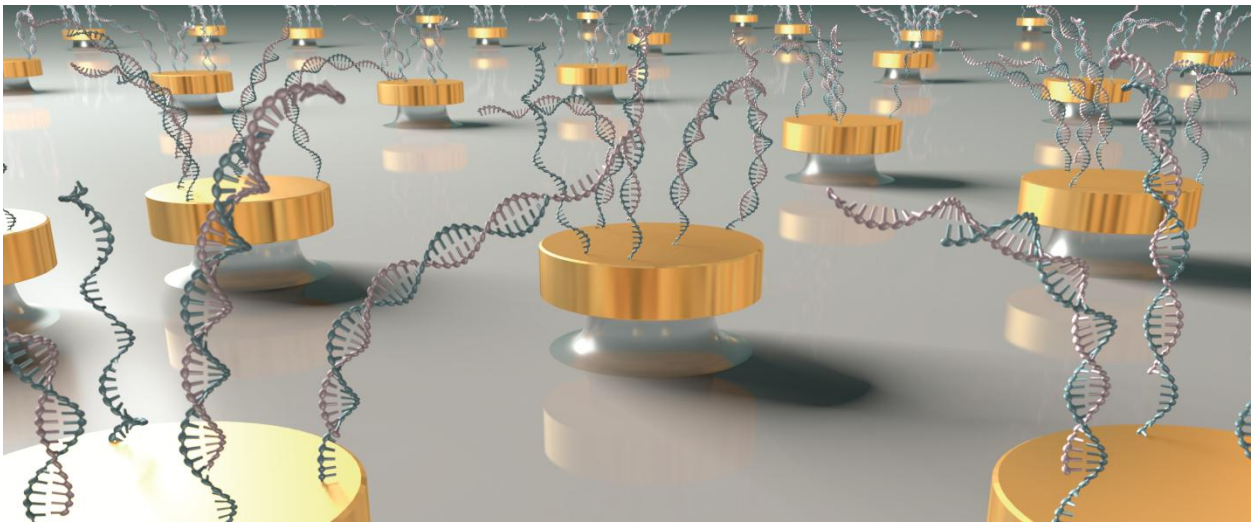

Figure 5

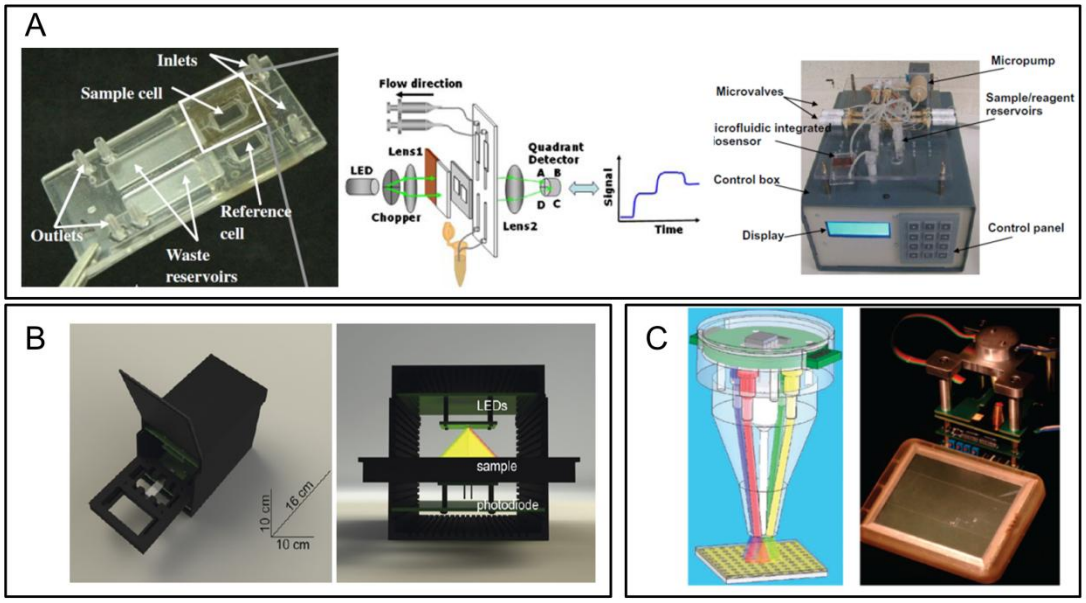
A
Inlets
Sample cell
Outlets
Reference cell
Waste reservoirs
Flow direction
Lens1
LED
Chopper
Quadrant Detector
A B
D C
Lens2
Signal
Time
Micropump
Microvalves
Sample/reagent reservoirs
Control box
Display
Control panel
B
10 cm
16 cm
LEDs
sample
photodiode
C

Figure 6